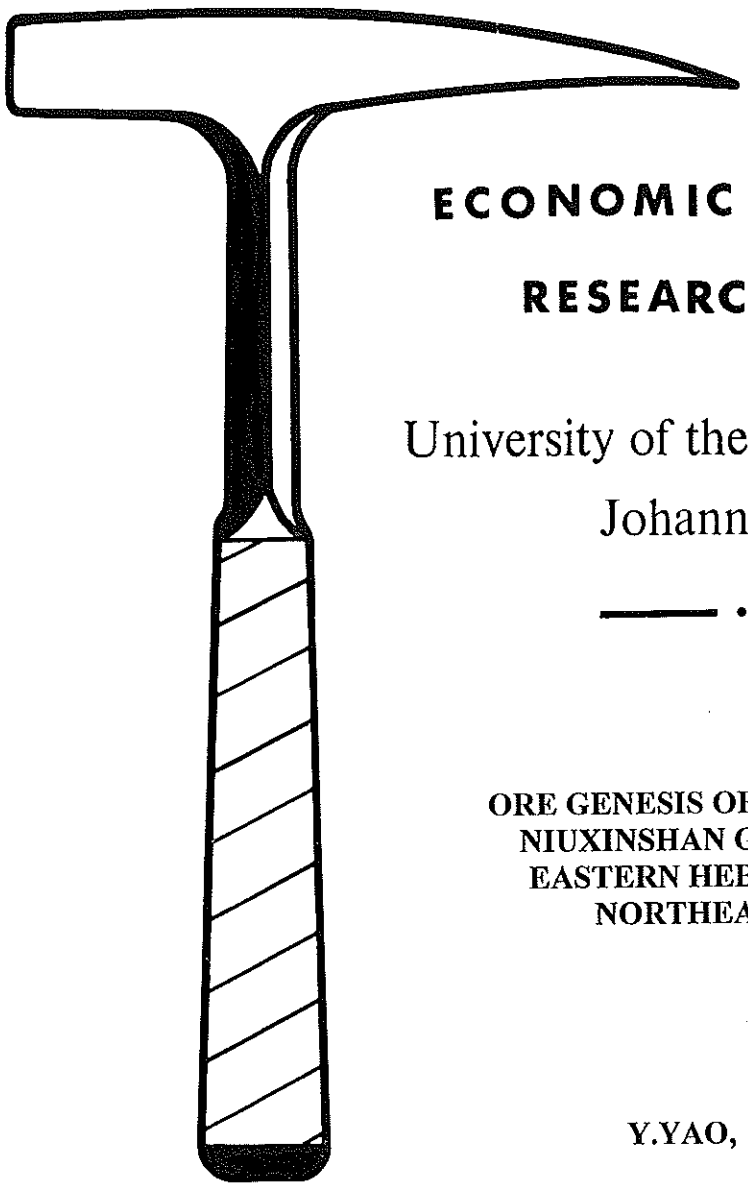

ECONOMIC GEOLOGY

RESEARCH UNIT

University of the Witwatersrand

Johannesburg

ORE GENESIS OF THE MESOZOIC NIUXINSHAN GOLD DEPOSIT, EASTERN HEBEI PROVINCE, NORTHEAST CHINA

Y.YAO, R.B.TRUMBULL, H.A.GILG and G.MORTEANI

INFORMATION CIRCULAR No. 331

UNIVERSITY OF THE WITWATERSRAND

JOHANNESBURG

ORE GENESIS OF THE MESOZOIC NIUXINSHAN GOLD DEPOSIT, EASTERN HEBEI PROVINCE, NORTHEAST CHINA

by

Y. YAO[1], R. B. TRUMBULL[2], H. A. GILG[3] and G. MORTEANI[3]

([1]: Present Address: Department of Geology, University of the Witwatersrand, P/Bag 3, WITS 2050, South Africa

2: GeoForschungsZentrum Potsdam, Projektbereich 4.2, Telegrafenberg A 50, D-14473 Potsdam, Germany

3: Lehrstuhl für Angewandte Mineralogie und Geochemie, Technische Universität München, Lichtenbergstr. 4, D-85747 Garching, Germany)

ECONOMIC GEOLOGY RESEARCH UNIT

INFORMATION CIRCULAR No. 331

February, 1999

ORE GENESIS OF THE MESOZOIC NIUXINSHAN GOLD DEPOSIT, EASTERN HEBEI PROVINCE, NORTHEAST CHINA

ABSTRACT

The Niuxinshan gold deposit is located near the eastern margin of the Archaean North China craton in eastern Hebei Province, and is a typical example of one of mainly mesothermal gold deposits, which formed during the Yanshanian (Jurassic to Cretaceous) tectono-magmatic reactivation of the craton. Gold-quartz veins are hosted mainly by Archaean amphibolites and also by the Mesozoic Niuxinshan granite stock. Four mineralization stages include: (1) quartz-K-feldspar; (2) quartz-pyrite; (3) quartz-polysulphide; and (4) quartz-carbonate. Gold is concentrated in stages 2 and 3. Hydrothermal alteration formed quartz-muscovite±pyrite±fluorite assemblages as vein haloes within the granite, and quartz-muscovite±pyrite-chlorite-carbonate assemblages within the amphibolites. In addition, K-feldspathization and/or fluoritization of the amphibolites is found locally near the granite contact. Mass balance calculations suggest that the mineralizing fluids removed Si and Na from both the granitic and the amphibolitic wall rocks, and added CO_2, F, S, K, and ore elements Au, Ag, Cu, Pb, Zn, W, Bi, and Mo to the two alteration zones. However, Ti, Al, Fe, Mg, V, Cr, Co, Nb, Ta and REE were buffered mainly by the wall rocks.

Fluid inclusions in fluorite from the greisen zones and in vein quartz and sphalerite from stages 1 to 3 are characterized by low to moderately saline (mainly 3 to 11 wt% NaCl equivalent) H_2O-CO_2 types, with XCO_2 values commonly from 0.1 to 0.4. The fluids in the inclusions evolved towards H_2O-enriched, and CO_2- and NaCl-poorer compositions through time. P-T conditions of the ore-forming fluids, constructed by isochores of the fluid inclusions, together with independent temperature-pressure constraints from alteration mineral assemblages and oxygen and sulphur isotope equilibrium thermometry, are at about 250 to 380 °C and 1 to 3 kbar for the stages 2 and 3.

$\delta^{13}C$ values of carbonates and fluid inclusion CO_2 in vein quartz from the stages 1 to 3 range from -6.3 to -2.5 ‰, and $\delta^{34}S$ values of sulphides cluster at 2.8 to 6.3 ‰. These are consistent with a magmatic-derived source for the carbon and sulphur. $\delta^{18}O$ values of sericite, quartz, K-feldspar and carbonates fall in a range from 8.4 to 15.8 ‰, corresponding to $\delta^{18}O_{H2O}$ values of 3.9 to 7.1 ‰ at 350 ± 50 °C; δD values of sericite range from -51 to -45 ‰; calculated δD_{H2O} values are between -26 and -20 ‰; measured δD_{H2O} values of fluid inclusions in quartz range from -85 to -64 ‰. The $\delta^{18}O_{H2O}$ and δD_{H2O} values suggest that the mineralizing fluids were mainly derived from a magmatic source. O-H isotope values of the fluids, calculated from the water/rock isotope exchange equilibrium, indicate a partial contribution of meteoric waters to the fluids.

Building on the geological setting, ore geology and geochemistry, fluid inclusions and stable isotopes of gangue minerals, it is suggested that the Niuxinshan gold deposit was formed mainly by magmatic-derived fluids with partial mixing of meteoric waters. Gold deposition was dominantly induced by decreases of temperature and pressure, and destabilization of the gold bisulphide complex during sulphidization of the wall rocks.

——— oOo ———

ORE GENESIS OF THE MESOZOIC NIUXINSHAN GOLD DEPOSIT, EASTERN HEBEI PROVINCE, NORTHEAST CHINA

CONTENTS

	Page
INTRODUCTION	1
METHODOLOGY	1
GEOLOGICAL SETTING	2
ORE GEOLOGY	4
NIUXINSHAN GRANITE	9
Petrology	9
Geochemistry	10
Isotopic Data	12
WALL ROCK ALTERATION	14
FLUID INCLUSIONS	18
Petrography	18
Microthermometric Results	21
STABLE ISOTOPES	25
Carbon Isotopes	25
Oxygen Isotopes	27
Hydrogen Isotopes	29
Sulphur Isotopes	29
DISCUSSION	30
P-T Conditions of Trapped Fluids	30
Source of Ore-forming Fluids	31
Gold Deposition	32
Genetic Model	34
CONCLUSIONS	34
ACKNOWLEDGEMENTS	35
REFERENCES	35

—— oOo ——

Published by the Economic Geology Research Unit
Department of Geology
University of the Witwatersrand
1 Jan Smuts Avenue
Johannesburg 2001
South Africa

ISBN 1-86838-240-0

ORE GENESIS OF THE MESOZOIC NIUXINSHAN GOLD DEPOSIT, EASTERN HEBEI PROVINCE, NORTHEAST CHINA

INTRODUCTION

Magmatic-related hydrothermal metallogeneses of (copper)-gold deposits have been studied by Burrows and Spooner (1987); Sillitoe (1989, 1991); Spooner (1991); Wyborn and Sun (1994); Hedenquist and Lowenstern (1994); and Hedenquist et al. (1996). It was suggested that the role of magmas in mineralization provided not only heat energy, but also magmatic fluids and components of metals and ligands (e.g. Hedenquist and Lowenstern, 1994), and that magnetite-series, I-type intrusions and sulphur-undersaturated magmas are associated with the Cu-Au mineralization (Sillitoe, 1991; Ohmoto, 1986; Wynborn and Sun, 1994).

The ore genesis of mesothermal lode gold deposits in Archaean greenstone terranes worldwide has been an active topic of debate for over a century. In general, a metamorphic model for the deposits has been preferred by many workers (e.g. Boyle, 1979; Ho, 1987; Groves and Forster, 1991; De Ronde et al., 1992; Kerrich, 1987, 1993; McCauig and Kerrich, 1994; Solomon and Groves, 1994; Witt et al., 1997), but a magmatic origin for the deposits was also proposed (e.g. Burrows et al., 1986; Burrows and Spooner, 1987; Hattori, 1987; Spooner, 1991). In addition, Nesbitt and Muehlenbachs (1989) concluded that mesothermal lode gold deposits in the Canadian Cordillera were generated by evolved meteoric waters, and Groves et al. (1998) considered that the lode gold deposits were produced orogenically.

Similarly, metallogenesis of hydrothermal gold-quartz vein deposits in eastern Hebei Province, which is one of the major areas hosting mesothermal gold mineralization in China, has also been contentious for many years. The controversy surrounding the genesis of the deposits includes the following models of origin: (1) metamorphic (Sun et al., 1989; Yang, 1989); (2) magmatic (Yu and Jia, 1989; Liu, 1989); (3) deep-seated hydrothermal (Bai et al., 1990; Zhang et al., 1991); (4) magmatic, with ore-bearing fluids mainly being derived from meteoric waters (Trumbull et al., 1992); and (5) orogenic (Miller et al., 1998). To assist with the gold exploration being conducted in eastern Hebei Province, a better understanding of genetic models for gold deposits in the area is especially useful. These models depend on further studies of the deposits on both a regional and a mine scale.

The Niuxinshan gold-quartz vein deposit is one of several major gold occurrences in eastern Hebei Province. The deposit is hosted in Archaean amphibolites and also in the Mesozoic Niuxinshan granite stock, two of the main rock types in the region. Hence, it was selected for a detailed gold metallogeny study. The purpose of this paper is to document the geological and geochemical characteristics of the gold-bearing ores, as well as the fluid inclusions and stable isotope data of the gangue minerals at Niuxinshan. These data, including the regional geological setting and the radiogenic age data of the mineralization, were compiled to evaluate the genesis of the Niuxinshan gold deposit.

METHODOLOGY

Fluid inclusion microthermometry was carried out on doubly polished sections (about 200 to 300 μm thick), using a Linkham TH 600 heating-cooling stage equipped with a Leitz microscope at the Technische Universität München, Germany. The SYNFLINC synthetic standards of CO_2 and H_2O fluid inclusions were used for calibration of the stage. Most measurements were made at a heating rate of 0.2 to 0.4 °C/min. as in calibration. Clathrate melting (Tmclat) was determined by temperature cycling (Roedder, 1963; Diamond, 1990),

and the heating rate near Tmclat was 0.1 to 0.2 °C/min. for measurement. The reproducibility of measurements was better than ± 0.2 °C below +30 °C and ± 2 °C at temperatures of total homogenization, where the chips were centred in the specimen holder. To control drift of the instrument, which was found to be significant at temperatures below -20 °C, the SYNFLINC CO_2 standard was measured daily for calibration during the cooling run.

Carbon and oxygen isotope analyses of carbonates, quartz, K-feldspar and sericite were performed with a Finnigan MAT 251 mass spectrometer also available at the Technische Universität München. Carbon and hydrogen isotope analyses of fluid inclusions in quartz and hydrogen isotope analysis of sericite were made with a VG-PRISM mass spectrometer at the Laboratoire de Sciences de la Terre, Ecole Normale Supérievre de Lyon, France. Carbon isotope values are reported relative to the PDB standard, and oxygen and hydrogen isotope values are reported relative to the SMOW standard. Sample preparations for isotope analysis are as follows:

(1) carbon isotope compositions of carbonates were analysed by the method of McCrea (1950). X-ray diffractometry (XRD) determined that carbonates (n=4) are ankerite and dolomite. Each sample was reacted with 100 % phosphoric acid in a glass tube in vacuum at 50 °C for 3 days, and the CO_2 was then extracted for carbon isotope analysis. Analytical reproducibility was better than ± 0.2 ‰ (2σ). For carbon isotope analysis of fluid inclusion CO_2 released from vein quartz (n=6), samples were degassed at about 180 °C for up to 3 days and heated at various temperature steps (100 to 350; 350 to 480; 480 to 550 °C) in a resistance furnace. The liberated gases (H_2O+CO_2) were collected with liquid N_2. The CO_2 gas was separated cryogenically with an ethanol plus N_2 mixture at -100 °C. Analytical reproducibility is better than ± 0.2 ‰ (2σ);

(2) the extraction of oxygen from quartz (n=12), sericite (n=7) and K-feldspar (n=3) for oxygen isotope analysis was made by the method of Clayton and Mayeda (1963). Samples were reacted with BrF_5 in nickel tubes at 500 °C in vacuum for 12 hours, and the liberated oxygen passed over hot graphite at 600 °C to convert it to CO_2. Analytical reproducibility is better than ± 0.2 ‰ (2σ); and

(3) hydrogen isotope analysis of sericite (n=4) was conducted by the method of Bigeleisen et al. (1952). Samples were degassed at 180 °C overnight in vacuum to remove absorbed water and subsequently heated with a resistance furnace to >1400 °C to liberate H_2O. The liberated H_2O was converted to H_2 by reaction with hot uranium at about 800 °C. Analytical reproducibility is better than ± 2 ‰ (2σ).

GEOLOGICAL SETTING

Eastern Hebei Province is one of the major areas of mesothermal gold mineralization in China and is situated near the eastern edge of the Sino-Korean platform, which is bordered on the northern margin by the Inner Mongolian Axis (Trumbull et al., 1992). The regional geology is characterized by basement-cored uplifts, which expose Archaean to early-Proterozoic amphibolite- and granulite-facies mafic and felsic orthogneisses and iron formation. The metamorphosed basement rocks are surrounded by unmetamorphosed continental marine sedimentary rocks of Middle Proterozoic to Cenozoic age. According to Bai et al. (1990), Zhang et al. (1991) and Trumbull et al. (1992), three geological stages in the area include: (1) basement formation from the Archaean to Early Proterozoic; (2) stable supracrustal development from the Middle Proterozoic to the Permian era; and (3) platform reactivation during the Mesozoic. The most intensive tectonic events in this area are part of the late Mesozoic Yanshanian (Jurassic to Cretaceous) orogeny, which forms regional E-W-; NE-SW-; and NW-SE-striking faults and fractures from an early to a late sequence. The first two phases produced regional tectonic, magmatic and mineralization zones (Figure 1),

whereas the NW-SE-trending fault zones are of small scale and are less important, regionally, to the gold mineralization.

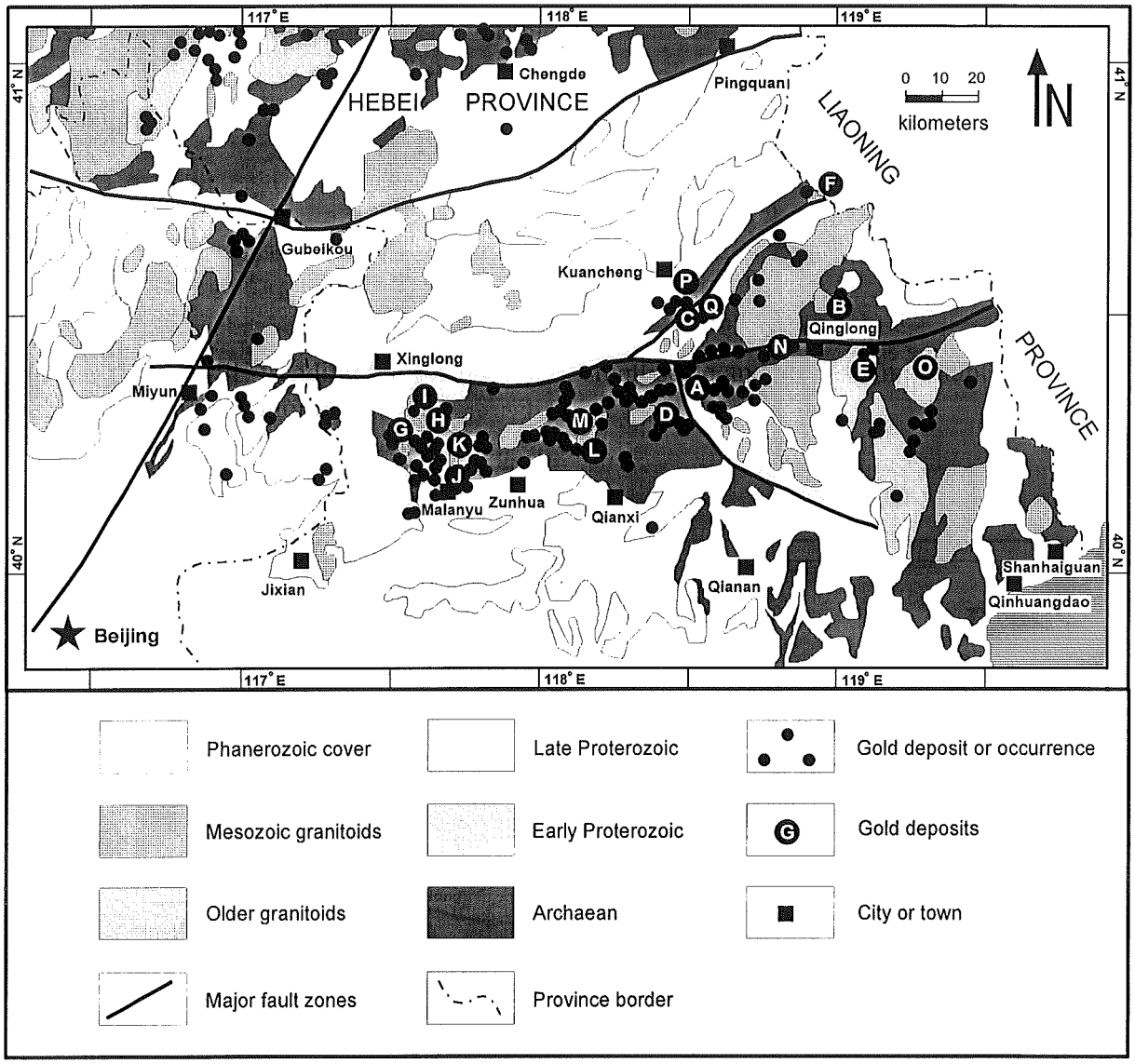

Figure 1. Simplified geological map of eastern Hebei Province with gold deposits and occurrences marked by black dots (modified from Bai et al., 1990; Trumbull et al., 1992). Large-sized gold deposit: D, Jinchangyu. Medium-sized gold deposit: ***A, Niuxinshan****; B, Sanjia; C, Yuerya. Small-sized gold deposit: A, Huajian; B, Wangtoushan and Xinglongou; D, Shangjiayu; E, Banbishan; F, Baizhangzi; G, Madi; H, Huashi; I, Daoliushui; J, Malanyu; K, Maoshan; L, Majiayu; M, Gaojiadian; N, Dachagou; O, Louzishan; P, Tangzhangzi; Q, Shanwanzi.*

Yanshanian granitoids and dykes extensively intruded the basement metamorphic rocks in eastern Hebei Province and are temporally and spatially associated with the regional gold mineralization (Figure 1). According to Yao (1997), the regional auriferous (n=10) and non-auriferous (n=12) granitoids show similarities in their petrography and geochemistry. The granitoids are mainly calc-alkaline in composition and consist of biotite-bearing (commonly <5 vol%) granites and hornblende-bearing (commonly 10 to 15 vol%) granodiorites. Accessory minerals mainly include magnetite, zircon, apatite, epidote, and sphene. The felsic granites are weakly peraluminous and metaluminous (ASI=0.9 to 1.2), but the granodiorites are moderately to weakly metaluminous (ASI=0.6 to 0.9). $\delta^{18}O$ values of 21 whole-rock granitoids range from 6.7 to 9.8 ‰ and initial Sr isotope ratios of 6 granitoids are between 0.704 to 0.707. The oxygen and strontium isotope data suggest that the regional granites are I-type intrusions and were probably generated by partial melting of infracrustal source materials (Yao, 1997, and references therein). Radiometric isotope ages of the granitoids from Rb-Sr, K-Ar, Pb-Pb and ^{40}Ar-^{39}Ar analyses (n=27) are concentrated at 130 to 190 Ma, with a range from 102 to 239 Ma, suggesting a dominantly Yanshanian period (Bai et al., 1990; Zhang et al., 1991). Field evidence demonstrated that gold-quartz veins post-dated the granitoids and granitic porphyry dykes, but pre-dated lamprophyre dykes (Bai et al., 1990).

Twenty one lode gold deposits and 235 gold occurrences in eastern Hebei Province have been reported (Bai et al., 1990; Trumbull et al., 1992). Gold-quartz veins are mainly hosted by Archaean amphibolites and less commonly by Mesozoic granitoids (Figure 1). The veins are controlled by NE-SW-trending secondary brittle faults and fractures. Three types of gold deposits have been reported (Bai et al., 1990). These include: (1) metamorphic rock-hosted (e.g. Jinchangyu, Sanjia); (2) granite-hosted (e.g. Yuerya, Wangtoushan); and (3) both metamorphic rock- and granite-hosted (e.g. Niuxinshan). Previous fluid inclusion studies of the major gold deposits (Jinchangyu, Niuxinshan, Yuerya, and Sanjia) showed that the gold-bearing fluids are low to moderately saline (4 to 9 wt % NaCl equivalent) H_2O-CO_2-bearing fluids, and minimum temperatures and pressures of ore formation were estimated to be at 250 to 350 °C and 1 to 2 kbar (Yu and Jia, 1989; Bai et al., 1990; Trumbull et al., 1992). Radiogenic isotope ages of gold ores for the four deposits cluster at 170 to 190 Ma, with a range from 130 to 230 Ma and coincide with the ages of regional granitoids.

On the basis of the geological setting, ore geology and geochemistry, fluid inclusions, stable isotopes and radiogenic ages of gangue minerals, it is suggested that the gold mineralization in eastern Hebei Province was formed by a similar mineralization process that was closely related to the regional Yanshanian tectono-magmatic event (Yu and Jia, 1989; Bai et al., 1990; Zhang et al., 1991; Trumbull et al., 1992; 1996; Yao, 1997; Miller et al., 1998).

ORE GEOLOGY

The Niuxinshan gold deposit is located about 200 km northeast of Beijing in eastern Hebei Province. Gold-quartz veins are mainly hosted by Archaean amphibolites and some veins also cut the Niuxinshan granite stock (Figure 2). The Archaean metamorphic rocks mainly consist of mafic and intermediate gneisses, migmatized amphibolites and mafic to felsic granulites. The host rocks were folded during the Precambrian and extensively faulted during the Mesozoic platform reactivation (Bai et al., 1990; Trumbull et al., 1992). The NE-SW-, E-W- and NW-SE-striking faults control the distribution of the Niuxinshan granite and dyke intrusions as well as the orientation of the quartz veins (Figure 2).

The Niuxinshan granite forms a small, zoned, NE-SW-trending stock and comprises a central white granite and an outer porphyritic red granite (Figure 2). Petrological and geochemical characteristics of the granite are described in a later section. On the southern

flank of the granite stock occurs a large body of breccia which was interpreted to be autolithic, formed by the abrupt release of magmatic volatiles at a relatively shallow level of intrusion (Bai et al., 1990; Trumbull et al., 1992). A greisen zone at the southeastern end of the breccia body (Figure 2) has not previously been described in detail, but has been sampled in exploration surveys and found not to contain significant gold values (Ministry of Metallurgical Industry, pers. comm.). In this paper the greisen (greisenization) referred to is confined to the relatively narrow zones of wall rock alteration in the granite body where it is

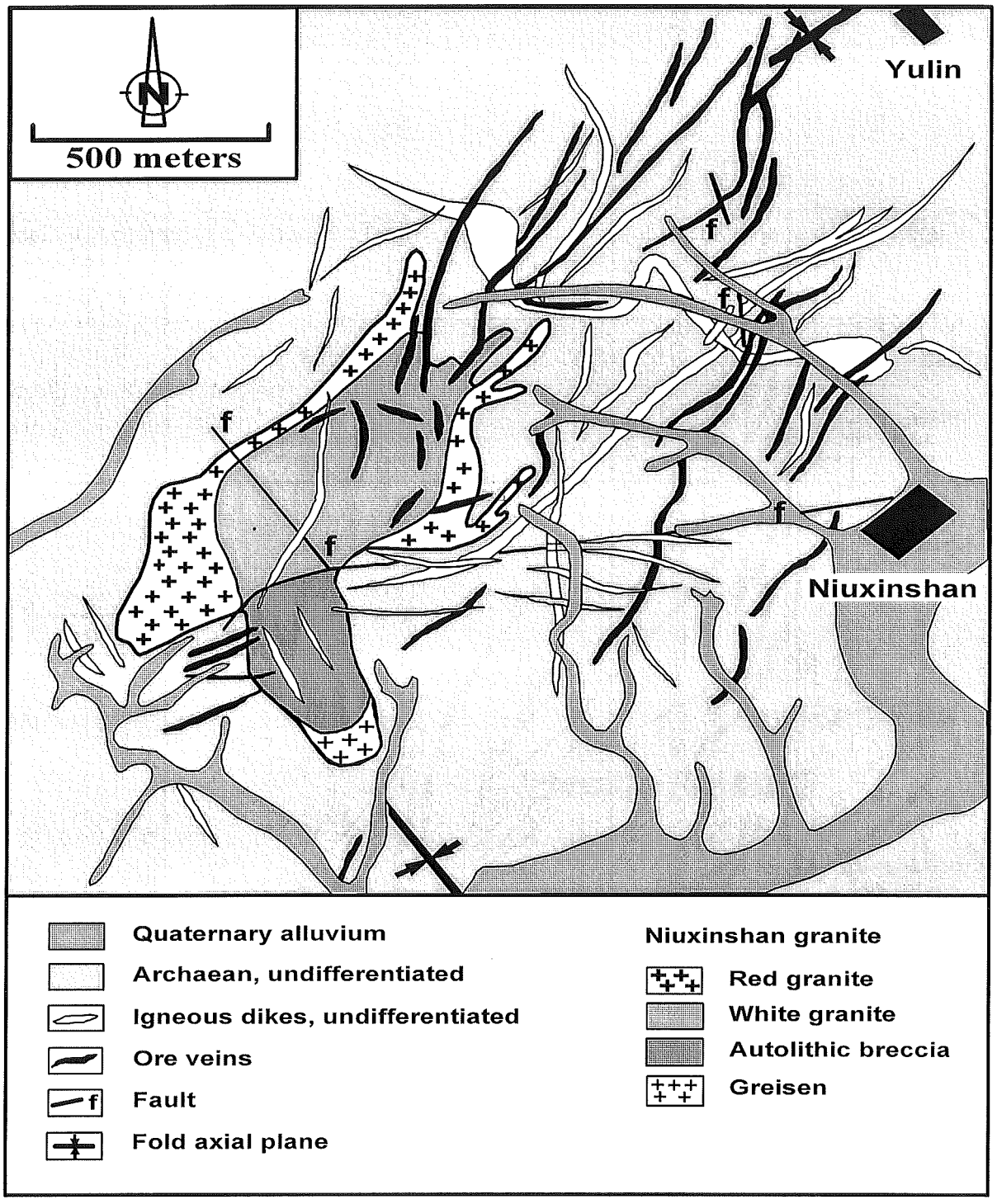

Figure 2. Simplified geological map of the Niuxinshan gold deposit (modified after Trumbull et al., 1992).

Table 1. Mineral assemblages and mineralization stages within the amphibolites from the Niuxinshan gold deposit, also showing temporal relationships of primary Tp1-P fluid inclusions with the stages (from Yao et al., 1999)

Stage		Stage 1 Quartz-K-feldspar	Stage 2 Quartz-pyrite	Stage 3 Quartz-polysulfide	Stage 4 Quartz-carbonate
Mineral					
Fluorite					
K-feldspar					
Chlorite					
Sericite					
Quartz					
Pyrite					
Native gold					
Scheelite					
Chalcopyrite					
Galena					
Sphalerite					
Native bismuth					
Dolomite					
Calcite					
Ankerite					
Fluid inclusion assemblages		Temporal sequence			
Composition	Generation				
H_2O-CO_2-type	Tp1-P-1q				
	Tp1-P-2q				
	Tp1-P-3q and Tp1-P-3s				

Note: Tp1-P: primary H_2O-CO_2 fluid inclusions, 1, 2 and 3 represent inclusions from stages 1, 2 and 3, respectively. q: quartz, s: sphalerite. In mineral assemblage lines, thick, moderate and fine bars represent major, minor and rare occurrences of minerals in each individual stage. In fluid inclusion lines, the bars denote temporal sequences of trapped inclusions during the mineralization stages. These are deduced from host minerals of fluid inclusions. For details see text.

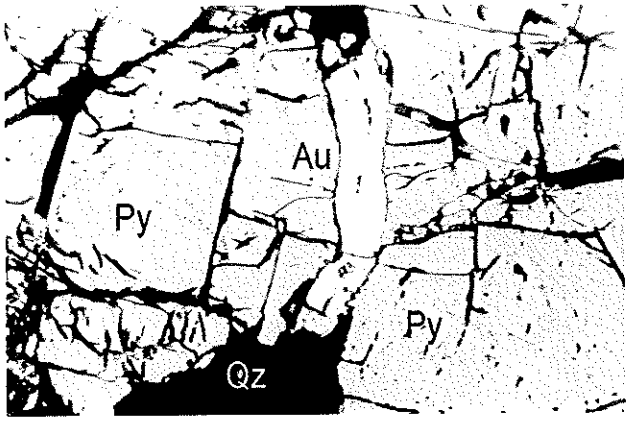

a: 6134, (width of view) WV=0.5 mm

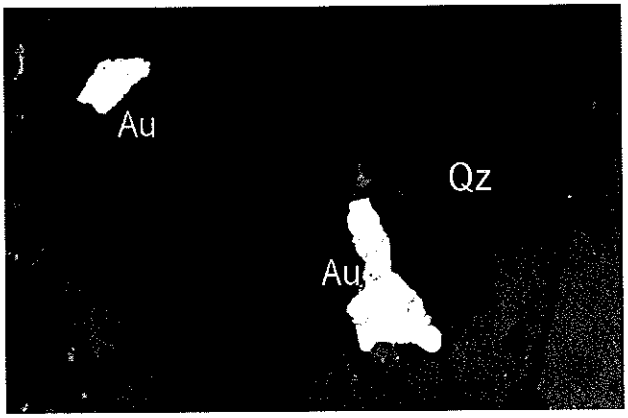

d: 6021, WV=0.5 mm

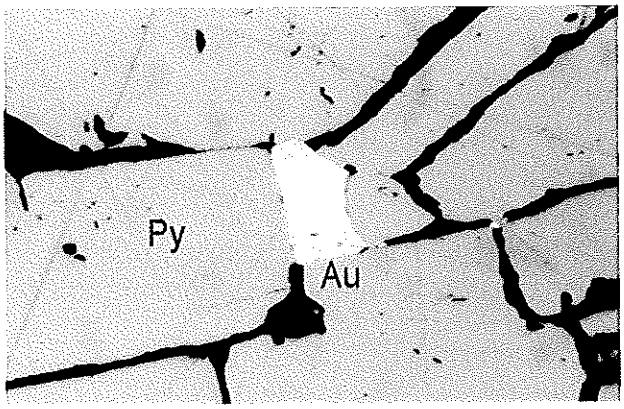

b: 6134, WV=0.2 mm

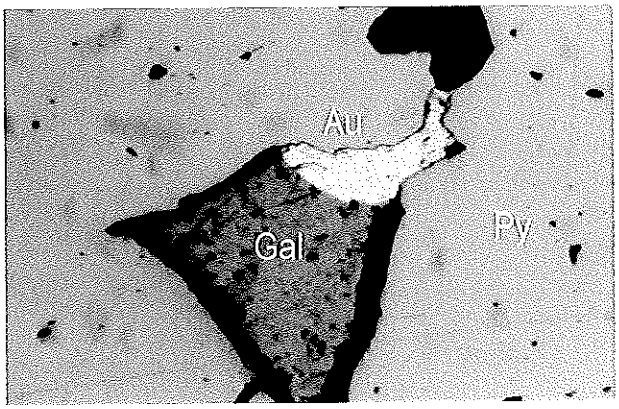

e: 6186, WV=0.2 mm

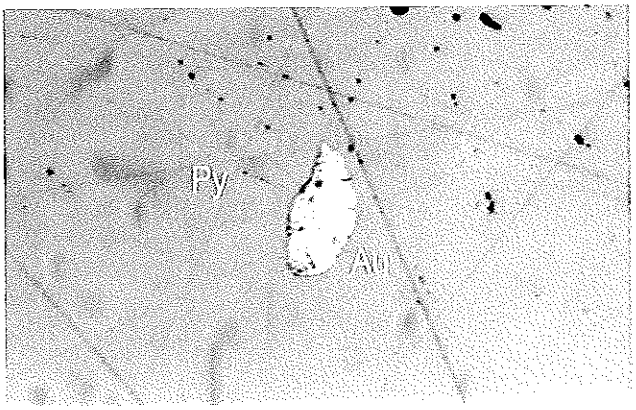

c: 6134, WV=0.2 mm

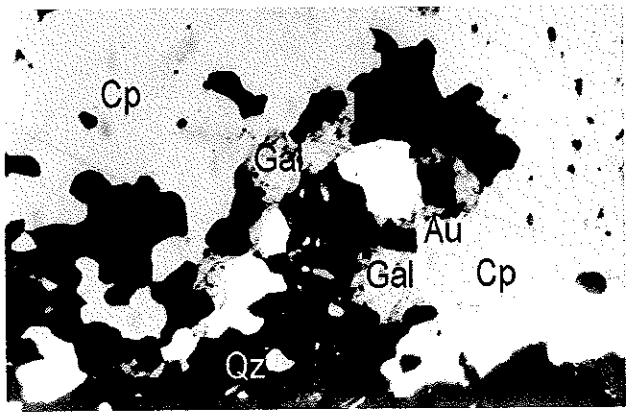

f: 6023, WV=0.5 mm

Figure 3. Photomicrographs of ores from the Niuxinshan gold deposit, showing native gold (Au). (a and d), gold in cracks in pyrite (Py) and quartz (Qz), (b and c), gold in pyrite grains, (e), gold intergrown with galena (Gal) in pyrite, and (f), gold intergrown with quartz and galena in chalcopyrite (Cp).

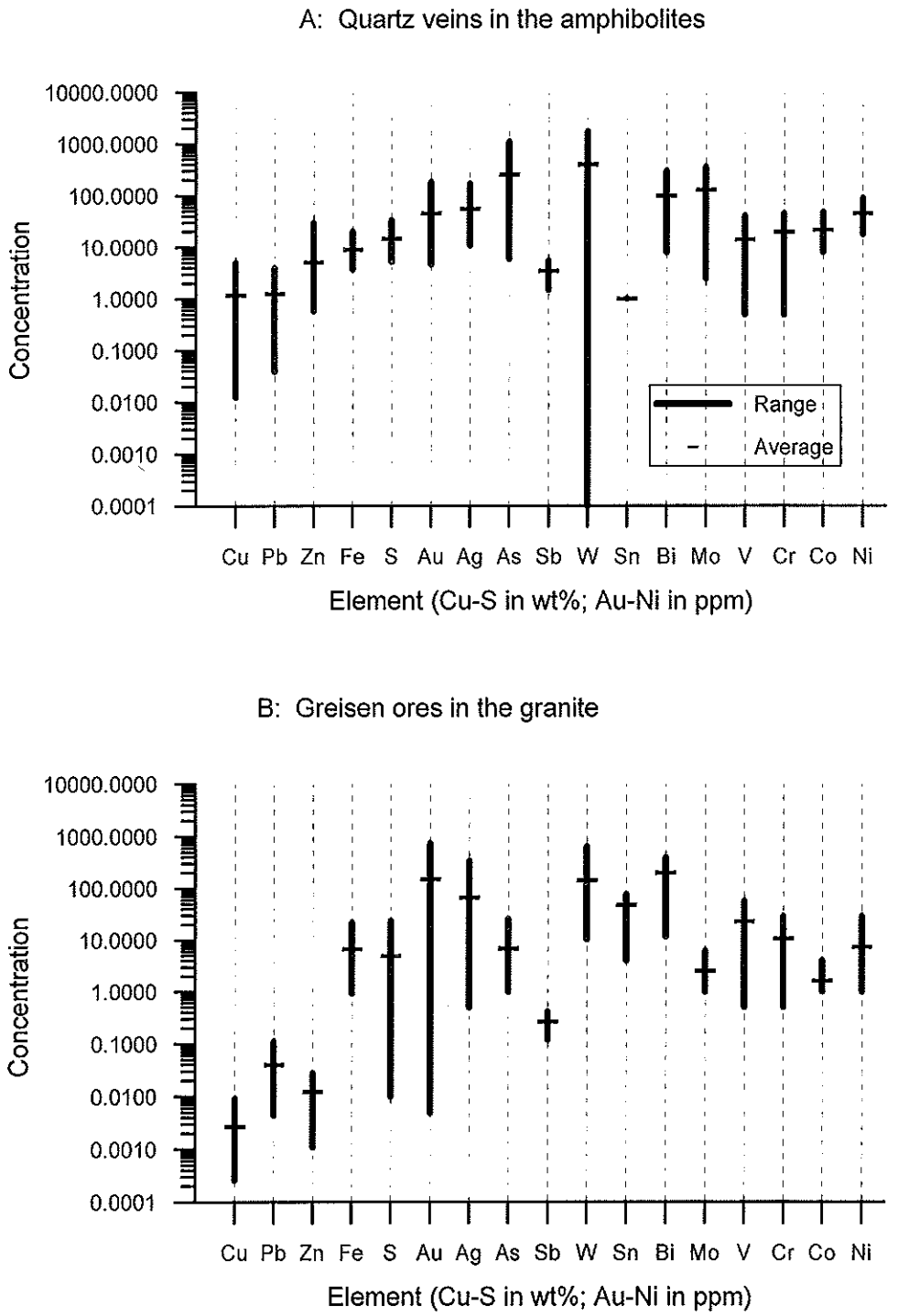

Figure 4. Histograms of element concentrations from selected ore samples in the Niuxinshan gold deposit.

transected by gold-quartz veins. A large number of igneous dykes occur within the granite and amphibolites. Cross-cutting relationships of the quartz veins with the granite and dykes indicate that the gold mineralization post-dated the intrusion of the Niuxinshan granite and porphyritic diorite dykes, but pre-dated the quartz trachyte and lamprophyre dykes (Bai et al., 1990).

Two types of gold mineralization can be distinguished according to the host rocks. The

more common type, and that which contains the bulk of the gold in the deposit, comprises gold-quartz veins within the Archaean amphibolites. The other, minor type comprises greisen alteration zones within the granite. The gold-quartz veins are mainly controlled by NE-SW-trending faults, are about 100 to 1000 m long, several decimeters to 2 m thick, and extend several tens of metres to 500 m in depth. Within the amphibolites, the quartz veins average 30 to 50 cm thick, whereas in the granite, the quartz veins are millimeters to centimeters thick (Bai et al., 1990; Trumbull et al., 1992).

Ore mineral paragenesis depends on mineralization type. In the amphibolites, the mineral assemblage consists of quartz and pyrite, with considerable base-metal sulphides (chalcopyrite, galena, sphalerite), traces of native gold, native bismuth, and scheelite. In the granite, the major ore mineral is pyrite, with trace native gold and rare base-metal sulphides. Because the mineralization in the granite is characterized by pervasively greisenized zones with quartz veins and veinlets, and is of minor importance economically (Trumbull et al., 1992), the mineral assemblages and mineralization stages shown in Table 1 pertain only to mineralization within the amphibolites. Four stages of mineralization (Table 1) are: (1) quartz-K-feldspar; (2) quartz-pyrite; (3) quartz-polysulphide; and (4) quartz-carbonate. The characteristics of each stage were described in detail by Yao (1997) and Yao et al. (1999). The gold mineralization is concentrated in stages 2 and 3. The gold occurs: (1) along microcracks within quartz and sulphides (mainly pyrite) (Figure 3a, b, d); (2) intergrown with sulphides (galena, sphalerite, chalcopyrite) and/or with quartz (Figure 3e, f); and (3) enclosed in sulphides (mainly pyrite) and quartz (Figure 3c). Types (1) and (2) constitute the main gold occurrences. Most of the gold is 0.1 and 0.3 mm in size and contains up to 35 wt% Ag (Trumbull et al., 1992).

Chemical compositions of ores from well-mineralized veins in the amphibolites and from greisen zones in the granite show a consistent element association of Au-Ag-Cu-Pb-Zn±(W-Sn-Bi-Mo) for the mineralization (Figure 4). The bulk Au/Ag ratios from both ore types span a wide range from 0.01 to 20 (n=14, Yao, 1997), which is attributed to the variable mineralogy of the bulk samples. The concentrations of base metals Cu, Pb, and Zn in amphibolite-hosted ores are individually greater than 0.1 wt%, and attain values of 5.0 wt% (Cu), 3.9 wt% (Pb) and 30.0 wt% (Zn). Base-metal contents in ores from the granite are individually all less than 0.1 wt%. The concentrations of W, Sn, Bi, and Mo are generally in the range of 10 to 1000 ppm from both types of ore.

The radiogenic age of mineralization, based on Rb-Sr and $^{40}Ar/^{39}Ar$ dating of hydrothermal K-feldspar, sericite and quartz, ranges from 175 ± 25 to 190 ± 2 Ma (Yu and Jia, 1989; Bai et al., 1990; Trumbull et al., 1992), and is comparable to the granite age of 174 ± 14 Ma. A K-Ar age of 166 Ma from a vein-cutting lamprophyre dyke (Sun et al., 1989) represents a minimum mineralization age.

NIUXINSHAN GRANITE

Petrology

The Niuxinshan granite is about 1000 m long and 400 m wide with an outcrop area of 0.35 km^2. The stock intruded the Archaean amphibolites and has an irregular shape with a NE-SW strike (Fig. 2). The red and white granites show similar mineral assemblages, mainly consisting of phenocrysts of quartz and feldspars with sizes in the range of 0.2 to 3 mm. The average CIPW normative mineral concentrations are 34% quartz, 34% plagioclase, and 30%

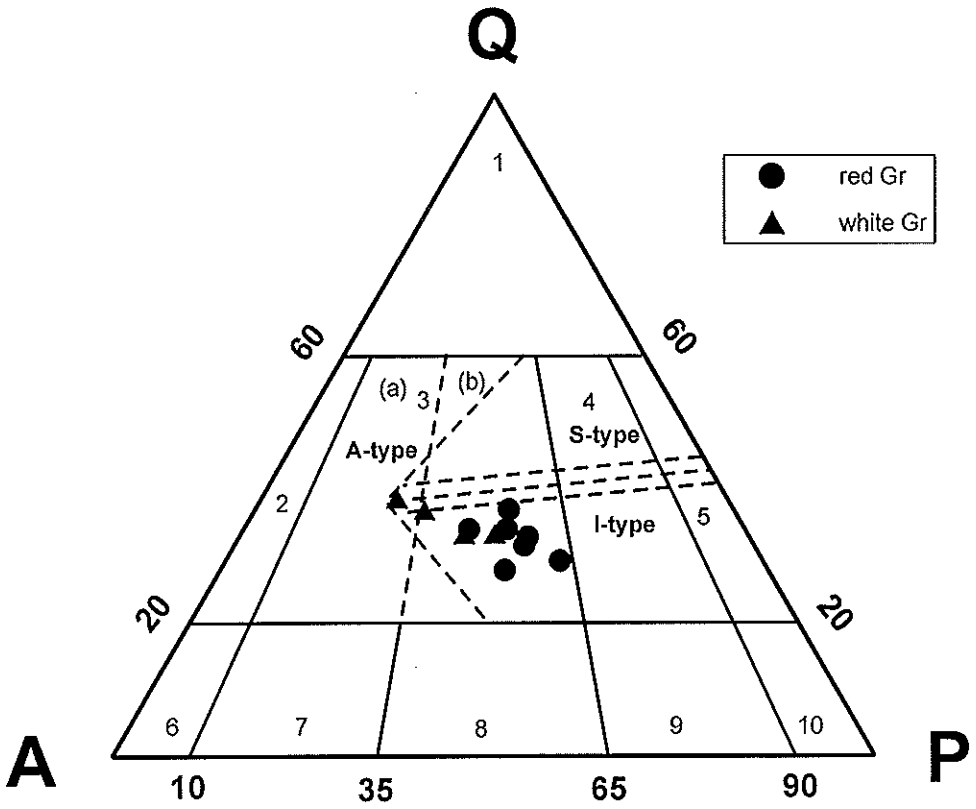

Figure 5. Ternary QAP diagram (Streckeisen, 1976) showing CIPW normative mineral compositions of the Niuxinshan granite. Q=quartz, A=alkali feldspar, P=plagioclase. Gr= granite. 1=quartz-rich granite, 2=alkali-granite, 3=granite, 3(a)=syenogranite, 3(b)= monzogranite, 4=granodiorite, 5=tonalite/trondhjemite, 6=alkali syenite, 7=syenite, 8= monzonite, 9=monzogranite/monzogabbro, 10=diorite/gabbro/anorthosite. Fields of S-, I- and A-type granites are from Whalen and Currie (1990).

K-feldspar, with rare biotite (<1 vol.%). Quartz forms allotriomorphic grains with undulatory extinction, and feldspars occur as allotriomorphic and (sub)euhedral plate crystals. K-feldspar shows microcline twinning and is more or less altered to clay minerals along twin planes. Plagioclase is commonly sericitized, particularly near quartz veins. Accessory minerals include white mica, zircon, allanite, apatite, magnetite and opaque minerals. The CIPW normative mineral compositions of both the red and white granites are similar and plot in the monzogranite field (Figure 5), and the field of I-type granite after Whalen and Currie (1990).

Geochemistry

The chemical compositions of both the white and red granites are similar and are characterized by high SiO_2 (73.5-76.3 wt%), total alkalis (K_2O+Na_2O) of 7.5-9.5 wt%, 12.7-13.9 wt% Al_2O_3, and very low contents of other oxides ($TiO_2+Fe_2O_3+MnO+P_2O_5$: 0.8 to 2.6 wt%). The aluminum-saturation index (ASI=molar $Al_2O_3/(Na_2O+K_2O+CaO)$ is between 0.9 and 1.2, and oxidation ($Fe_2O_3/(Fe_2O_3+FeO)$) values range from 0.3 to 0.6, which shows that the granite is weakly metaluminous to mildly peraluminous, and moderately oxidized. In comparison with the average granite composition of Vinogradov (Rösler and Lange, 1972),

the trace element contents of the Niuxinshan granite show slightly higher Rb; higher W, Sn, Bi, Mo, Ag, and Zn; lower S, F, Sr, Ba, V, Cr, Co, Ni, Li, Cs, Zr, and REE; and nearly the same Au, As, Sb, Be, U, and Y concentrations (Yao, 1997).

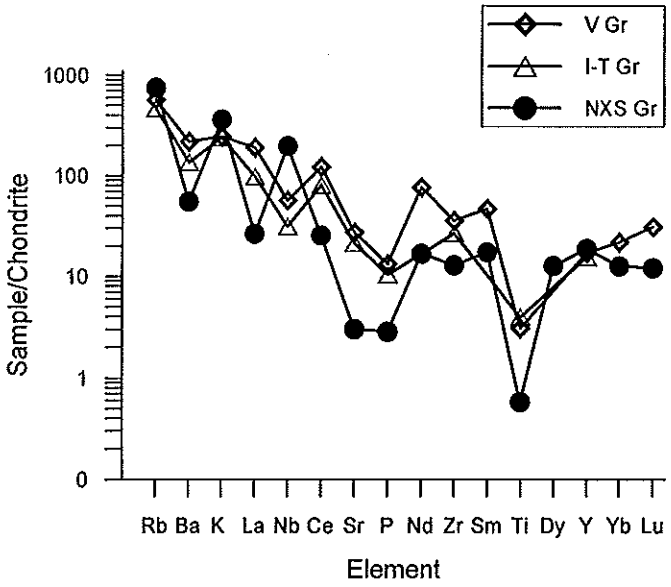

Figure 6. Normalized abundance pattern of incompatible elements for the Niuxinshan granite (NXS Gr) compared with average V Gr granite (Vinogradov) from Rösler and Lange (1972) and I-T Gr granite (I-type) from Chappell and White (1992). Normalization values are from Sun (1980) and Jahn et al. (1980).

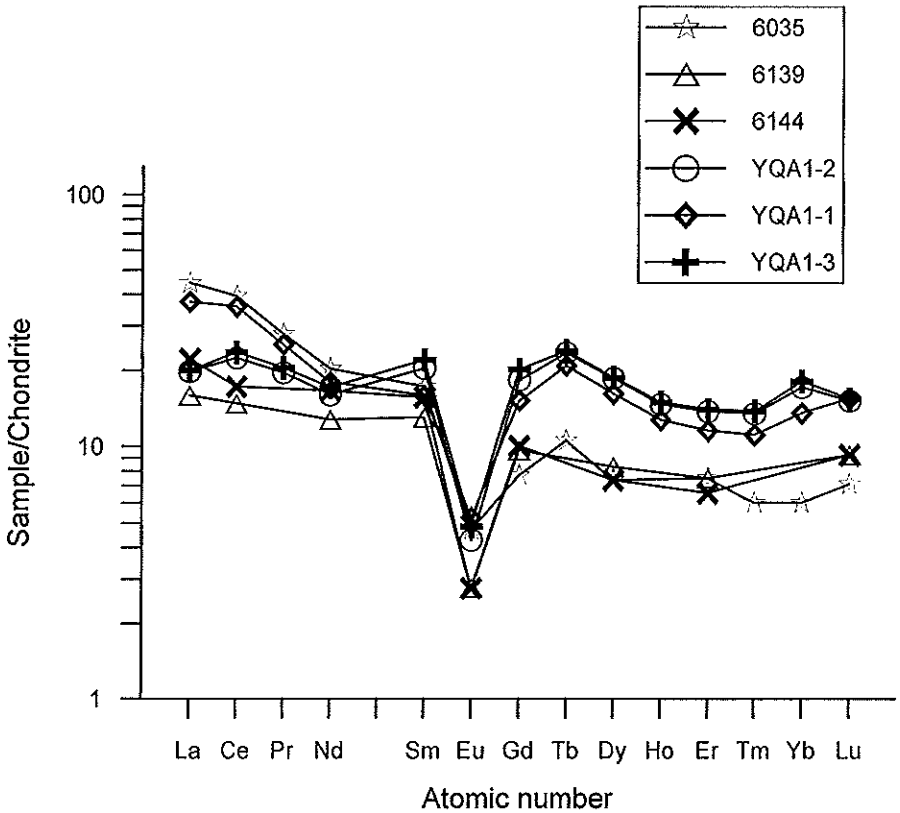

Figure 7. Chondrite-normalized REE distribution patterns from least altered samples of the Niuxinshan granite.

The chondrite-normalized incompatible element pattern (Figure 6) is characterized by high Rb, K, Nb, and low REE concentrations, and shows similarities to those of Vinogradov and I-type granites, except for more positive Nb and more negative Ba, La, Sr, P, and Ti anomalies. Negative Nb anomalies of granites were attributed to low primary concentrations (Briequeu et al., 1984; Dada et al., 1995). However, Nb is characterized by high concentrations in "within plate granite" (Pearce et al., 1984). Thus, the positive Nb anomaly of the Niuxinshan granite may reflect its tectonic setting as part of a stable craton. The Ba, La, Sr, P, and Ti anomalies reflect a higher degree of fractionation than the Vinogradov and I-type granites.

The chondrite-normalized REE distributions are regular and flat with a moderate negative Eu anomaly (Eu/Eu*=0.2 to 0.4) (Figure 7), which suggests low to moderate fractionation. Two REE distribution patterns are evident: (1) higher LREE than HREE normalized abundances (6035, 6139, 6144); and (2) nearly equal LREE and HREE (YQA1-1, -2, -3). The different REE patterns, especially the LREE depletion and the HREE enrichment, may imply an evolution of the magma from an early to late stage (Yao, 1997).

Isotopic Data

Oxygen isotope compositions of quartz and K-feldspar from the least altered granite are shown later in Table 3. The $\delta^{18}O$ values of quartz range from 10.6 to 11.2 ‰ (n=3), and the $\delta^{18}O$ values of co-existing K-feldspar in each sample are between 11.2 and 12.9 ‰, indicating that the primary igneous $\delta^{18}O$ values have been changed by extraneous fluids at relatively low temperature (O'Neil, 1986). This is supported by the microscopic characteristics of K-feldspar, which shows slight alteration to clay minerals even in the fresh granite. The oxygen isotope compositions of quartz from weakly to strongly altered granite are similar, reflecting less influence of hydrothermal fluids on quartz than K-feldspar. Zhang et al. (1991) concluded that the $\delta^{18}O$ values of quartz are about 1.7 ‰ greater than those of the whole-rock granites in the Jinchangyu district. Based on this value and the measured $\delta^{18}O$ values of quartz, the $\delta^{18}O$ values of the Niuxinshan whole-rock granite are between 8.9 and 9.5 ‰, which are comparable to that of I-type granite (< 10 ‰, Chappell and White, 1992).

Pb isotope compositions of the Niuxinshan granite, dykes, ores and regional Archaean amphibolites are compiled from Bai et al. (1990), Yu and Jia (1989), Yu et al. (1989), and Zhang et al. (1991), and are plotted in Figures 8 and 9. The Pb isotope compositions of the Niuxinshan granite and K-feldspar are similar to those from the ores, and their $^{206}Pb/^{204}Pb$, $^{207}Pb/^{204}Pb$, $^{208}Pb/^{204}Pb$ values show little variation, but are different to the dykes and regional Archaean amphibolites. The dykes show more radiogenic whole-rock lead than the granite which may imply that the dykes contain more U and Th concentrations than the granite, or that the dykes were derived from a source with richer lead isotope compositions than granite-derived materials. These two possibilities cannot be discussed further because of lack of U and Th analyses and no detailed petrogenetic data for the dykes. In addition, the Archaean amphibolites have the lowest Pb isotope compositions. Yu and Jia (1989), and Trumbull et al. (1992) suggested that the ore lead was derived, at least in large part, from the uranium-depleted metamorphic basement. Similarly, Bai et al. (1990) and Zhang et al. (1991) proposed that the lead of ores and granites was derived from deep-seated sources.

The calculated single-stage ages for the granite and ores are much older than the Mesozoic ages of granitic emplacement and mineralization (Fig.8). The lead isotope compositions from the ores and granite contain very non-radiogenic lead for their age, and this rules out comformable and single-stage lead. As shown in Figure 8, all the lead compositions, except for some points from the dykes, plot near the mantle accretion curve ($\mu \approx 7.8$), which indicates that the lead could be derived from uranium-depleted mantle sources.Figure 9 shows

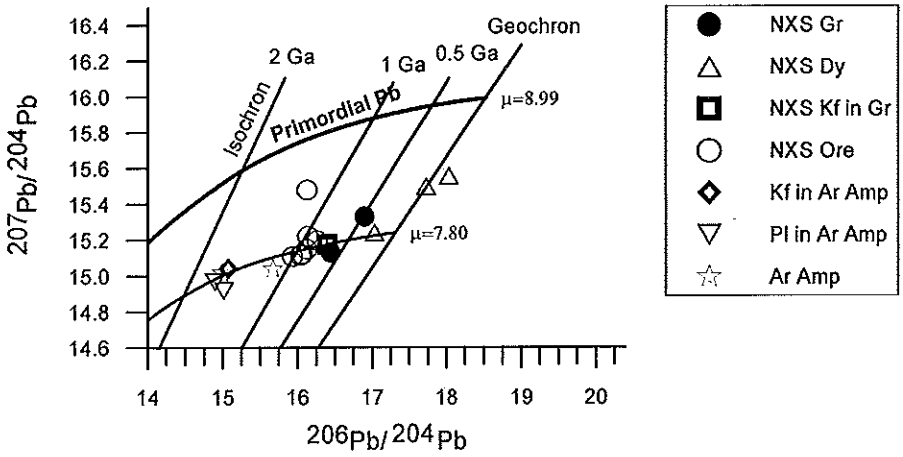

Figure 8. Present-day Pb-Pb diagram for the Niuxinshan granite, ores and dykes with the 4.55 Ga geochron and selected isochrons calculated from Doe and Zartman (1979). For comparison Pb isotopic compositions from the regional Archaean amphibolites are also shown. NXS=Niuxinshan, Ar=Archaean, Gr=granite, Dy=dyke, Kf=K-feldspar, Pl=plagioclase, Amp=amphibolites.

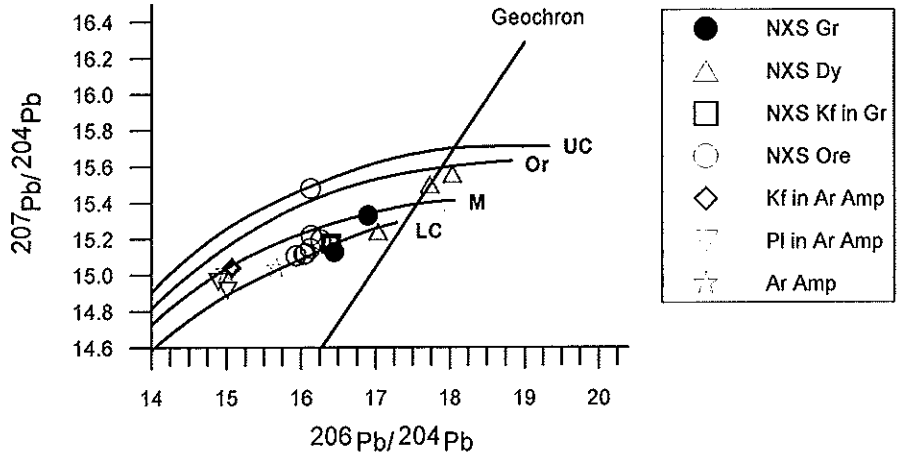

Figure 9. Diagram of Pb isotopic compositions for the Niuxinshan granite, ores and dykes in the plumbotectonic model of Zartman and Doe (1981) and Doe and Zartman (1979) with the 4.55 Ga geochron. M=mantle, LC=lower crust, Or=orogenic crust, UC=upper crust. For comparison Pb isotopic compositions from the regional Archaean amphibolites are also shown. Abbreviations as in Figure 8.

that most of the lead compositions are distributed between the lower crust and mantle Pb curves in the plumbotectonic model of Zartman and Doe (1981), and Doe and Zartman (1979). Taking into account the Sr and O isotopes of the granite, it is suggested that the lead of the ores and granite was derived from the uranium-depleted lower crust. The Yanshanian orogeny thus resulted in a high degree of homogeneity of lead isotope compositions (Yao, 1997).

A Rb-Sr isochron age has been reported to be 174±14 Ma, with initial $^{87}Sr/^{86}Sr$ ratio of 0.704±0.004 for the white granite, which supports the field observations and indicates the Yanshanian age of the granite (Bai et al., 1990). The low initial $^{87}Sr/^{86}Sr$ ratio suggests that

the granite was generated by infracrust-derived source materials (Chappell and White, 1992). This is also consistent with the Pb isotope data of the granite.

In summary, the petrological, geochemical, and isotopic (O, Pb, Sr) data suggest that the Niuxinshan granite is an I-type intrusion and may have been derived from the partial melting of infracrustal source materials, which were not involved in a weathering cycle (Chappell and White, 1992; Trumbull et al., 1996). The potential magma source may be derived from partial melting of igneous rocks from the lower crust, which may be, at least partially, related to the Archaean basement metamorphic rocks at depth (Yao, 1997).

WALL ROCK ALTERATION

The wall rocks were altered along and/or near the margins of quartz veins both in the amphibolites and the granite. The alteration is irregular in shape, and generally shows zoning symmetric to the veins. In the weak and strong alteration zones, being away from and near the veins, the alteration type and mineral assemblage are different and never spatially reversed, which is well suited for a study of wall rock alteration.

In the granite, the alteration zone extends for over one metre in thickness and is characterized by an inner greisenization (muscovite+silica)±fluorite±pyrite and an outer sericitization zone. Carbonatization is only locally found. The least altered granite grades into sericite-dominated rocks, with the alteration increasing toward the veins. Sericite is only found in plagioclase and in the matrix as fine-grained aggregates. K-feldspar and quartz are very weakly altered, and the primary granite fabric is preserved. Near the greisen zone, plagioclase

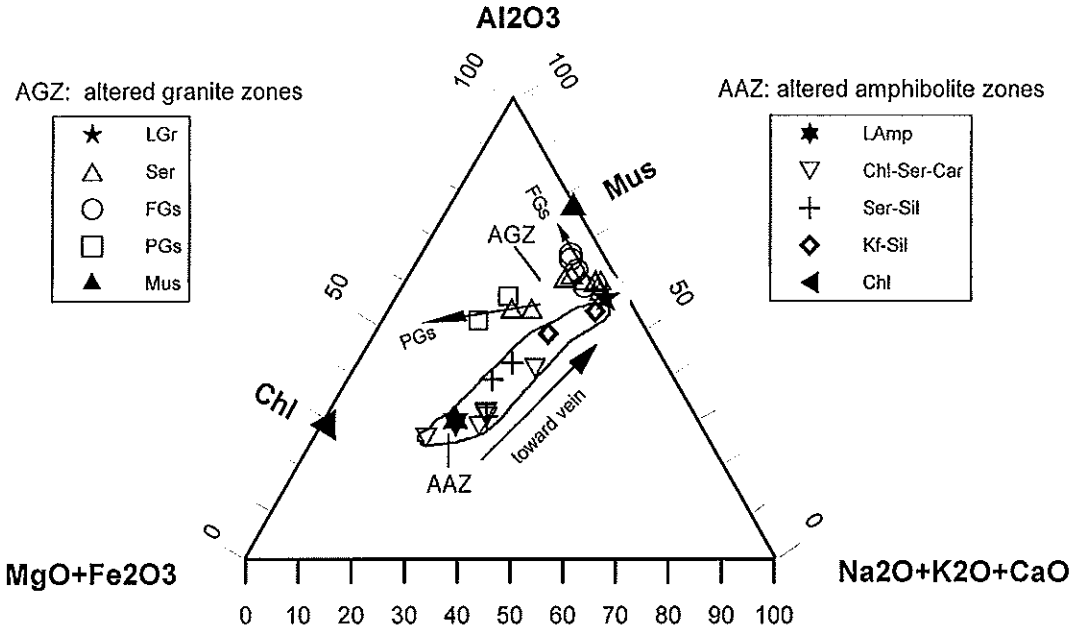

Figure 10. Ternary diagram of Al_2O_3-($MgO+Fe_2O_3$)-(Na_2O+K_2O+CaO) in wt% showing compositions of the altered granite and amphibolite zones. LGr=least altered granite, Ser=sericitization, FGs=greisenization with fluorite, PGs=greisenization with pyrite, Mus=muscovite, Chl=chlorite, Ser=sericite, Car=carbonate, Sil=silicification, Kf=K-feldspar. Lamp= the least altered amphibolites. AGZ=altered granite zone, AAZ=altered amphibolite zone.

and K-feldspar are replaced mainly by flakes or large patches of sericite. In the most intense cases of alteration, plagioclase is completely replaced by pseudomorphs of sericite. The greisen zone is about 10 to 30 centimetres wide near the edges of veins. The primary granite fabric is completely destroyed, and the original minerals are almost entirely replaced by muscovite, secondary quartz, fluorite and, locally, pyrite. Muscovite occurs as large plate aggregates up to 2 to 3 mm in size. Some secondary quartz exists as pseudomorphs of feldspar, and primary quartz is rarely preserved. Fluorite is commonly present in paragenesis with secondary quartz. Locally, pyrite may amount to more than 50 vol% of the altered rock, which then constitutes high-grade greisen gold ores up to 733 g/t Au (Yao, 1997).

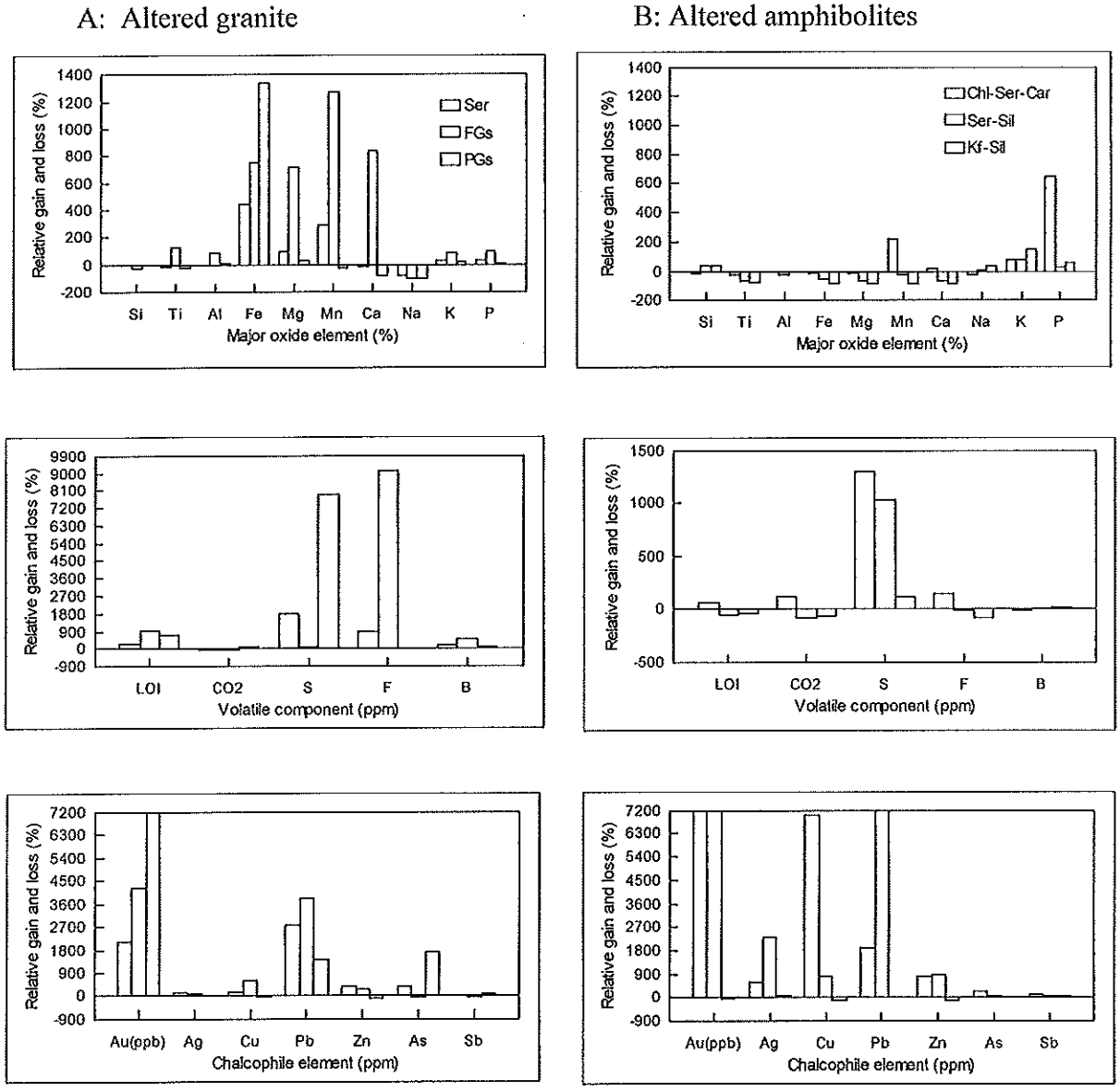

Figure 11. Diagrams of relative gains and losses of chemical components from the altered granite and amphibolite zones. Ser=sericitization zone, FGs=greisenization zone with fluorite, PGs=greisenization zone with pyrite. LOI=loss on ignition. Chl-Ser-Car= chloritization-sericitization-carbonatization zone, Ser-Sil=sericitization-silicification zone, Kf-Sil=K-feldspathization-silicification zone.

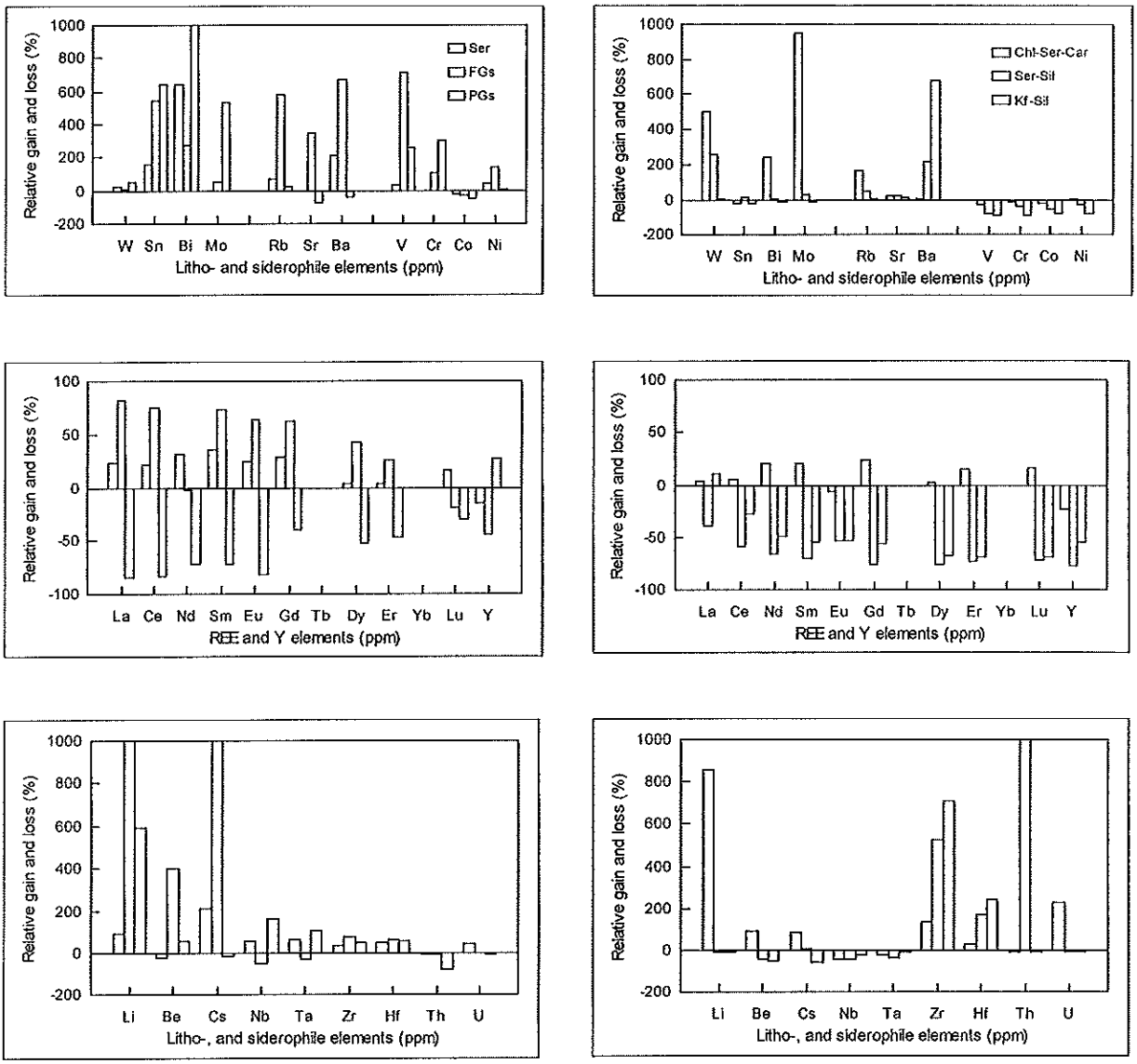

Figure 11. (continued).

In the amphibolites, alteration zones commonly attain thickness of several to tens of centimetres and show intense decoloration from dark green to light grey near the quartz veins. The alteration mainly comprises an inner silicification+sericitization±pyritization and an outer sericitization+chloritization+carbonatization zone. The least altered amphibolites are characterized by minor fine-grained aggregates of chlorite and sericite in both hornblende and plagioclase. With alteration increasing towards the veins, biotite and hornblende are replaced by chlorite, and plagioclase is replaced by sericite. Finally, sericite itself is gradually replaced by chlorite and carbonates. Furthermore, secondary quartz gradually increases, and carbonates, as fine-grained aggregates and later stage veinlets, are commonly formed. Sulphides (mainly pyrite) occur to a minor extent in the altered rocks. The sericitization-silicification zone is closest to the veins and consists of large amounts of sericite and hydrothermal quartz with minor late-stage chlorite and carbonates. Sulphides (mainly pyrite) are minor in abundance. Near the granitic contact, K-feldspathization and fluoritization are locally found.

In a plot of all major oxides except silica (Figure 10), compositions of the sericitized and greisenized zones in the granite demonstrate a trend toward muscovite with alteration, whereas compositions of the greisen with pyrite and some sericitized rocks move to the Fe_2O_3+MgO end point, due to the abundance of pyrite (Figure 10). In the amphibolites, compositions of the altered rocks generally evolve toward muscovite (sericite) (Figure 10). These are consistent with the mineralogical characteristics of the alteration zones described above.

Figure 11 shows average relative gains and losses of chemical compositions in the alteration zones from the two wall rocks (Yao, 1997). Because calculated values of samples from the same alteration type show similar trends to relative gains and losses, as well as the net transfer of chemical components, only the average results are plotted in Figure 11. A large amount of Si and all the Na are depleted in the alteration zones. Ti, Mn, and Ca decrease in the greisen zone with pyrite, but increase in the greisen zone with fluorite. Al, Fe, Mg, K, and P are largely gained (Figure 11A). Destruction of plagioclase and K-feldspar causes depletion of Si and Na. The net transfer of Si and Na across the alteration zones is -6614 and -20783 g/m^3, respectively. Due to the formation of muscovite, fluorite and pyrite, Al, Fe, Mg, Mn, Ca, K, Ti, and P are enriched in the alteration zones. Except for slight increases of CO_2 and B components, LOI, S and F show strong enrichments; the net transfer of S and F is 1315 and 8213 g/m^3, respectively. Loss on ignition largely increases due to H_2O-bearing muscovite. The formation of fluorite causes intense enrichment of F. The gains of S mainly depend on the formation of pyrite, B may be partially distributed in muscovite and CO_2 is related to carbonates. Apart from the decrease of Co, and partial decrease of Sr, Ba, Be, Nb, Ta and Th, the chalco-, litho- and siderophile elements are characterized by enrichments. Au, Ag, Cu, Pb, Zn, Sn, Bi and Mo are especially enriched. The net transfer of Au and Ag through the alteration zones averages 1.4 and 1.3 g/m^3, respectively. REE elements are generally enriched in the sericitization and greisenization zones with fluorite, but depleted in the greisenization zones with pyrite. Y decreases in the sericitization and greisenization zones with fluorite, but increases in the greisenization zones with pyrite. The net transfer of these elements through the alteration zones is very slight.

In the alteration zones of the amphibolites, K and P are enriched, whereas Ca and Mn are depleted. The concentrations of K are closely related to sericite and K-feldspar relics. However, Si, Ti, Al, Fe, Mg, and Na are strongly depleted. The net transfer of Si, Fe, Mg, and Na through the alteration zone is -20873, -41679, -29358, and -3237 g/m^3, respectively. The volatile components of LOI, CO_2, B and S are largely enriched due to the formation of sericite, chlorite, carbonates and pyrite. Au, Ag, Cu, Pb, Zn, W, Bi, Mo, Rb, Sr, Zr, Hf, and Th are characterized by strong enrichment. The net transfer of Au and Ag averages 0.8 and 4.5 g/m^3, respectively. The net transfer of Cu, Pb, and Zn through the alteration zone is 2494, 511 and 4101 g/m^3, respectively. In contrast, Sn, V, Cr, Co, Ni, Nb, and Ta are largely depleted (Figure 11B). REE elements shows slight increases in the chloritized-sericitized-carbonatized zones, but large depletions in the sericitized and K-feldspathized zones (Figure 11B).

According to petrographic and geochemical characteristics and fluid inclusion data (see below) from the altered granite and amphibolite haloes, a model of infiltration and diffusion for fluid-rock alteration is proposed (Figure 12). It is suggested that the alteration fluids in proximal wall-rock alteration zones were similar to the vein fluids in major fluid components (e.g. CO_2, S, Fe, Na, Ca, K, Au, Ag, Cu, Pb, Zn), but buffered by the rocks in minor fluid components (e.g. Ti, Mg, Al, P, V, Cr, Co, Ni, REE). Figure 12 shows a model of a fault system, as well as vein and alteration haloes in the granite and amphibolites. The externally derived H_2O-CO_2-NaCl fluids brought components such as CO_2, S, K, and ore-bearing metals into the rocks and ascended along faults and structures through the granite and amphibolites The fluids interacted with the wall rocks through infiltration and diffusion from the veins to

the wall rocks. The different primary wall rock lithologies resulted in the exchange and redistribution of components (e.g. Ti, Fe, Al, Mg, REE) in the alteration haloes. The fluid infiltrated along microfractures and small veinlets producing alteration zones extending from the veins to the wall rocks. The diffusion normal to the veins resulted in compositional changes in the altered haloes, which is indicated by the mass balance calculations.

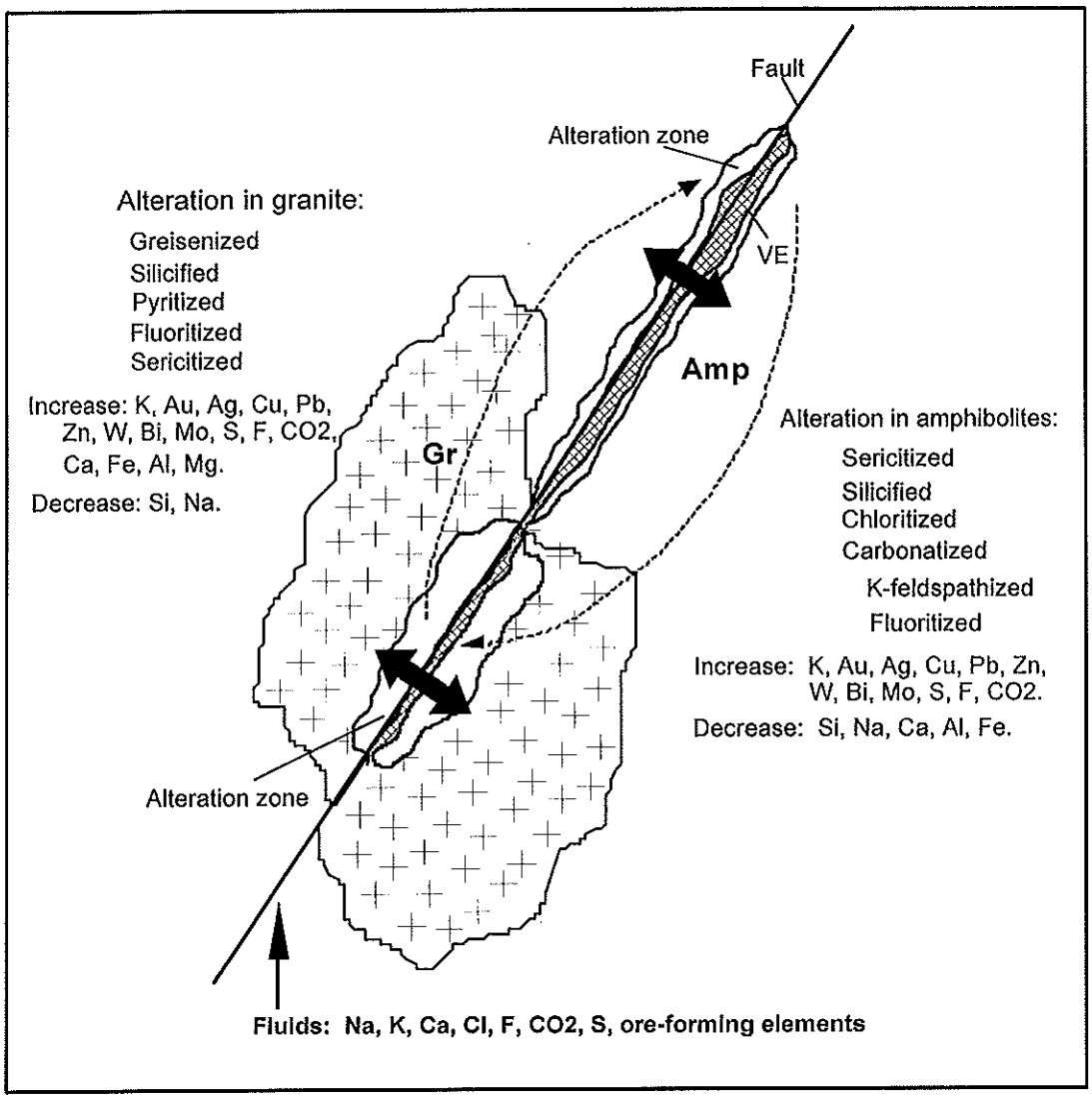

Figure 12. Hypothetical model of infiltration and diffusion alteration from vein fluids to the granite and amphibolites. Gr=granite, Amp=amphibolites.

FLUID INCLUSIONS

Petrography

Fluid inclusions in fluorite from the greisen zones and in vein quartz and sphalerite from stages 1 to 3 on 10 doubly polished sections (about 200 to 300 μm thick) were studied. According to Yao (1997), three compositional types of fluid inclusions were recorded:

(1) primary (Tp1-P) and secondary (Tp1-S) H_2O-CO_2-NaCl inclusions with two or three phases at 25 °C. They are present in all the samples studied. The Tp1-P inclusions are 3 to 23

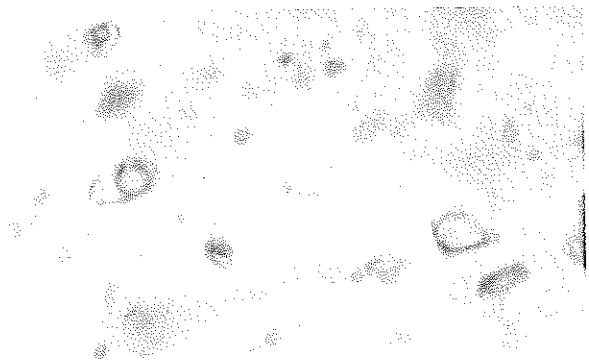

a: 6181, WV=0.09 mm

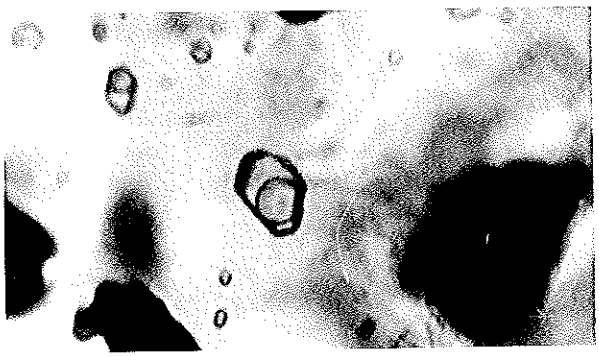

d: 6018d, WV=0.09 mm

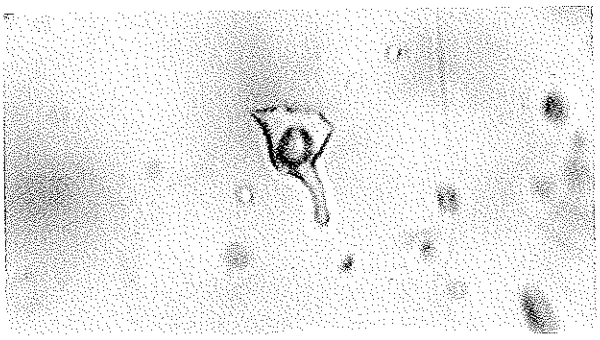

b: 6018c, WV=0.09 mm

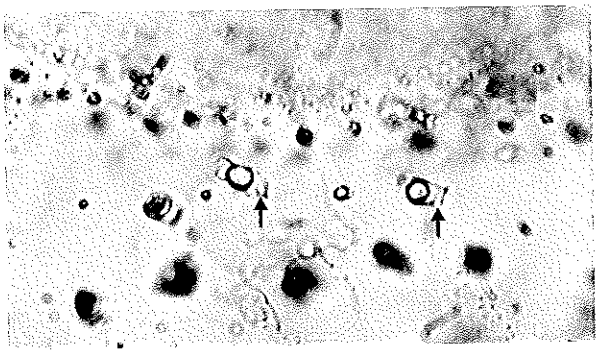

e: 6145, WV=0.09 mm

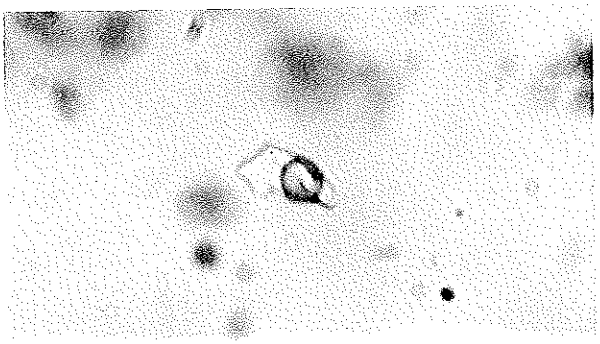

c: 6018c, WV=0.09 mm

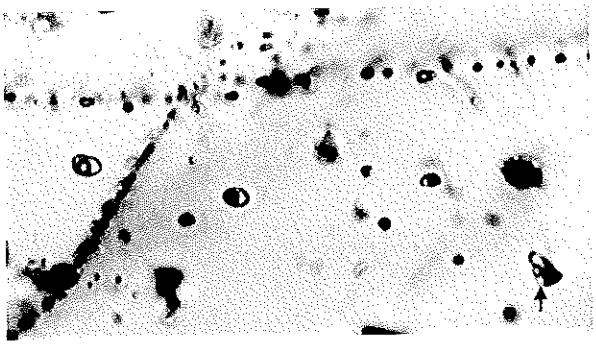

f: 6145, WV=0.2 mm

Figure 13. Photomicrographs of fluid inclusions in the Niuxinshan gold deposit. WV=width of view. a-d. Primary type 1 H_2O-CO_2 fluid inclusions showing 2- (a, b, d) or 3-phases (c) at room temperature (CO_2 vapour, CO_2 liquid and aqueous liquid) in quartz (a-c) and sphalerite (d) from quartz-K-feldspar stage 1 (a) and quartz-polysulphide stage 3 (b-c). Note inclusions with moderate and high CO_2 volume ratios from stage 1 in a, and the long, narrow, shape of inclusion due to necking-down from stage 3 in b. e-f. Secondary Tp1-S (H_2O-CO_2) and Tp2-S (H_2O-CO_2-daughter crystal carbonates) inclusions along microcracks or grain boundaries in fluorite from greisen zones in the granite. Note small daughter crystals (bright points directed by arrows).

μm in the longest dimension, and occur in isolated forms or in intragranular groups with other compositionally similar inclusions (Figure 13c-f); in some cases, inclusions in vein quartz from stage 3 show evidence of necking-down (Figure 13b). Based on temporal sequences of their host minerals, the Tp1-P inclusions can be subdivided into the following groups: (1) Tp1-P-1q with variable VCO_2 (0.1 to 0.9) in vein quartz from stage 1; (2) Tp1-P-2q with VCO_2 (commonly 0.4 to 0.6) in vein quartz from stage 2; (3) Tp1-P-3q with VCO_2 (commonly 0.2 to 0.5) in vein quartz from stage 3; (4) Tp1-P-3s with low VCO_2 (0.2 to 0.4) in vein sphalerite from stage 3. Tp1-P-Gq and -Gf are defined by host minerals quartz and fluorite, respectively, from the greisen zones (G). The inferred temporal relationships between inclusion groups and mineralization stages are shown in Table 1. The Tp1-S inclusions in fluorite show relatively low VCO_2 of 0.2 to 0.4, and are about 2 to 15 μm in length with various shapes. They are aligned along microcracks of fluorite and cut growth planes of fluorite. The inclusions coexist with the Tp2-S (Figure 13g, h) in fluorite;

(2) secondary (Tp2-S) H_2O-CO_2-NaCl inclusions commonly with a small (<3 μm in size) and irregular solid phase (Figure 13h) in fluorite. The solid phase shows high birefringence and is thought to be carbonate. The inclusions are about 5 to 15 μm in size, and occur along healed microcracks of fluorite grains, together with Tp1-S inclusions (Figure 13g, h). Similarities of microthermometric data of the Tp2-S (with solid phases) and the Tp1-S (without solid phases), and the fact that the solid phase does not melt, even at 500 °C, suggest that the solid phase may represent accidental entrapment rather than a true daughter mineral (Yao et al., 1999); and

(3) secondary (Tp3-S) aqueous two-phase inclusions with a small bubble of less than 10 vol% at 25 °C. Most of the Tp3-S inclusions in vein quartz and sphalerite from the amphibolites are generally <3 μm in size, contain no solid phase, and are too small to measure microthermometrically. However, Tp3-S inclusions in fluorite from the greisen zones are commonly >5 μm in size, with a small birefringent (carbonate?) solid phase, and coexist with Tp2-S inclusions.

Microthermometric Results

Microthermometric results of the fluid inclusions studied are shown in Table 2 and plotted in Figures. 14 to 16.

Tp1-P inclusions show XCO_2 values of 0.06 to 0.76, with an average of 0.12 to 0.30 for inclusions in minerals of the different mineralization stages (Table 2). Final melting temperatures of solid CO_2 ($TmCO_2$) span a range from -59.6 to -56.8 °C (Figure 14A-E). In most cases, $TmCO_2$ values are more than 1 °C below the triple point of pure CO_2 (-56.6 °C), indicating the presence of additional volatile species (CH_4, N_2). In all cases, homogenization temperatures of carbonic phases into liquid ($ThCO_2(L)$) range from 7.4 to 31 °C and cluster at 22 to 28 °C (Figure 15A-E), corresponding to CO_2 densities of 0.51 to 0.88 g/cm^3. Assuming that the depression of CO_2 melting temperatures is caused by CH_4, mole fractions of CH_4 (XCH_4) were estimated by the measured $TmCO_2$ and $ThCO_2(L)$ temperatures (Thiéry et al., 1994). The estimated XCH_4 values are mostly between 0.003 and 0.03, with an average of 0.008 to 0.02 for inclusions in minerals of the different mineralization stages (Table 2). Melting temperatures of CO_2-clathrate (Tmclat) in the inclusions range from 2.1 to 9.8 °C and generally increase from the Tp1-P-G to Tp1-P-3s inclusions. Bulk salinities of the inclusions estimated from the Tmclat are between 0.4 and 12.5 wt% NaCl equivalent and decrease from the Tp1-P-G to Tp1-P-3s inclusions (Figure 22). Total homogenization temperatures of inclusions are designated as (Thtot), whereas Th(L) and Th(V) represent the homogenization of inclusions into the aqueous fluid phase and the CO_2 gas phase, respectively. Except for the

Table 2. Summary of microthermometric data for measured fluid inclusions in the Niuxinshan gold deposit (after Yao et al., 1999)

Host Mineral	Sample	Type	Description	Alteration/ stage	Size micron		$TmCO_2$ °C	Tmclat °C	$ThCO_2(L)$ °C	Th(L) °C	Th(V) °C	Salinity wt% NaCl	VCO_2 %	VCO_2-C %	XH_2O	XCO_2	XNaCl	XCH_4	DCO_2 g/cm^3	Db g/cm^3	Vb cm^3/mole
Fluorite	6143	Tp1-P-Gf	FGr	GZG	2-15	Ave	-58.4	4.5	27.5	336	331	9.6	40		0.78	0.18	0.03	0.01	0.72	0.92	26.90
						Sd	0.2	0.6	2.1	67	n.s.	0.9	13.8		0.09	0.09	0.003	0.008	0.05	0.04	4.3
						N	21	21	21	16	3	21	22		18	18	18	18	18	18	18
Quartz	6142c	Tp1-P-Gq	FGr	GZG	5-23	Ave	-58.5	5.1	22.5	322		8.7	53		0.70	0.26	0.02	0.02	0.74	0.89	29.53
						Sd	0.3	0.4	3.4	26		0.6	14		0.12	0.11	0.004	0.008	0.04	0.05	4.6
						N	23	23	23	23		23	23		23	23	23	23	23	23	23
Quartz	6038	Tp1-P-Gq	PGr	GZG	2-7	Ave	-58.1	5.7	23.9	313		7.8	52		0.72	0.23	0.02	0.02	0.72	0.88	29.10
						Sd	0.5	0.8	5.4	25		1.3	11.7		0.10	0.11	0.002	0.007	0.06	0.04	3.2
						N	12	12	12	12		12	12		12	12	12	12	12	12	12
Quartz	6181	Tp1-P-1q	KVA	Stage 1	2-12	Ave	-58.3	6	23.2	313	317	7.6	56		0.66	0.30	0.02	0.02	0.73	0.87	31.54
						Sd	0.4	0.5	4.2	39	35.6	0.9	18		0.15	0.15	0.004	0.012	0.05	0.06	6.1
						N	92	91	92	61	32	89	97		89	89	89	89	89	89	89
Quartz	6021	Tp1-P-2q	PVA	Stage 2	3-22	Ave	-58.2	5.8	24.7	310		7.7	52		0.72	0.24	0.02	0.02	0.71	0.87	29.42
						Sd	0.5	0.7	3.5	30		1.2	14		0.12	0.11	0.004	0.010	0.06	0.05	4.7
						N	12	12	12	12		12	12		12	12	12	12	12	12	12
Quartz	6152	Tp1-P-2q	PVA	Stage 2	2-8	Ave	-58.1	5.1	23.9	325		8.7	57		0.67	0.29	0.02	0.02	0.72	0.87	31.32
						Sd	0.6	0.5	2.6	32		0.8	14		0.12	0.13	0.004	0.012	0.04	0.05	5.1
						N	22	22	22	22		22	22		22	22	22	22	22	22	22
Quartz	6018c	Tp1-P-3q	QSA	Stage 3	2-10	Ave	-57.7	6.8	26.6	301		6.1		41	0.79	0.19	0.02	0.008	0.68	0.89	27.39
						Sd	0.6	1	2.4	28		1.8		20	0.16	0.17	0.006	0.011	0.04	0.08	8.0
						N	104	104	115	91		104		80	80	80	80	80	80	80	80
Sphalerite	6018d	Tp1-P-3s	QSA	Stage 3	5-16	Ave	-58.3	7.3	25.6	269		5.1		32	0.86	0.12	0.02	0.007	0.7	0.92	23.79
						Sd	0.2	0.6	2.7	23		1.1		9.9	0.07	0.03	0.003	0.005	0.04	0.05	3.9
						N	52	52	64	53		53		49	49	49	49	49	49	49	49
Fluorite	6145a	Tp1-S-Gf	FGr	GZG	2-15	Ave	-58.3	7.6	25.1	267		4.5		27	0.89	0.09	0.01	0.007	0.71	0.94	22.66
						Sd	0.3	0.2	2.1	25		0.4		7.2	0.03	0.03	0.001	0.002	0.03	0.03	1.5
						N	24	24	24	24		24		24	24	24	24	24	24	24	24
Fluorite	6145a	Tp2-S-Gf	FGr	GZG	2-15	Ave	-58.3	7.7	25.5	253		4.5		22	0.91	0.07	0.01	0.005	0.7	0.95	21.59
						Sd	0.2	0.27	1.3	15		0.5		7.3	0.03	0.03	0.03	0.002	0.02	0.03	1.3
						N	16	16	16	16		16		16	16	16	16	16	16	16	16
Fluorite	6145b	Tp3-S-Gf	FGr	GZG	2-20	Ave				180		4.1								0.92	20.14
						Sd				34		1								0.04	0.8
						N				18		18								18	18

Note: $TmCO_2$=melting temperature of carbonic phase, Tmclat=melting temperature of clathrate, $ThCO_2(L)$=homogenization temperature of carbonic phase into carbonic liquid, Th(L)=total homogenization temperature of inclusions into aqueous fluid, Th(V)= total homogenization temperature of inclusions into carbonic fluid. Salinity=salinity in wt% NaCl equivalent, VCO_2=CO_2 volume ratios visually estimated at room temperature, VCO_2-c=calibrated CO_2 volume ratios after Schwartz (1989). X=mole fraction of components of H_2O, CO_2, NaCl and CH_4. XCH_4 was estimated from the vX diagram of the binary CO_2-CH_4 system (Thiéry et al., 1994). DCO_2=density of carbonic phases in inclusions, Db=density of bulk fluid inclusions, Vb=bulk molar volume of inclusions. n.s.=no standard deviation calculation, due to small measured numbers. Tp1-P=primary H_2O-CO_2 fluid inclusions. 1, 2 and 3 represent inclusions from stages 1, 2 and 3, respectively, whereas G stands for inclusions from the greisen zones in the granite. q=quartz, s=sphalerite, f=fluorite. Tp1-S=secondary H_2O-CO_2-bearing inclusions, Tp2-S=secondary H_2O-CO_2-bearing inclusions with a solid phase, Tp3-S=secondary H_2O-rich inclusions with a solid phase. FGr=greisen with fluorite in the granite, PGr=greisen ore with pyrite in the granite, KVA=quartz-K-feldspar vein in the amphibolites from stage 1, PVA=quartz-pyrite vein in the amphibolites from stage 2, QSA=quartz-polysulfide vein in the amphibolites from stage 3, GZG= greisen zones in the granite. Calculations of fluid density, salinity, mole fractions of H_2O, CO_2 and NaCl, and molar volume were made using the FLINCOR program of Brown (1989).

Tp1-P-1q inclusions, most of the Tp1-P inclusions homogenized into aqueous fluid (Th(L)).

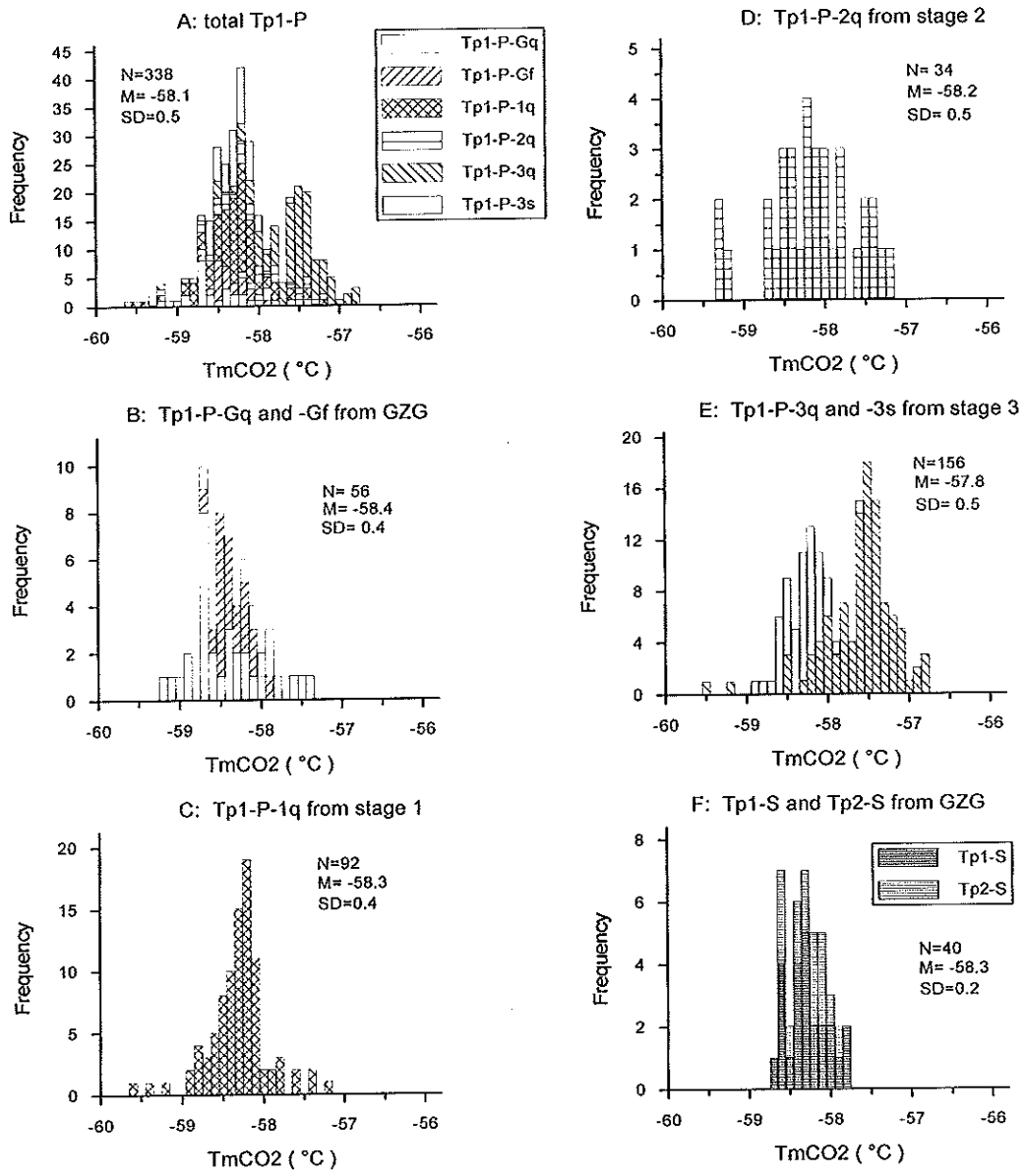

Figure 14. Frequency-$TmCO_2$ histograms from fluid inclusion microthermometric data. $TmCO_2$=melting temperature of carbonic phases. Tp1-P=primary H_2O-CO_2 inclusions, subscripts from -1q to -3s denote relative generations from stages 1 to 3 veins in the amphibolites, q=quartz, s=sphalerite. Tp1-P-G=primary H_2O-CO_2 inclusions from greisen zones in the granite, subscripts q and f represent inclusions in quartz (q) and fluorite (f), respectively. GZG=greisen zones in the granite. Tp1-S=secondary H_2O-CO_2 inclusions in fluorite from the greisen zones, Tp2-S=secondary H_2O-CO_2 inclusions with a solid phase (carbonates?) in fluorite from the greisen zones. N=number of measured inclusions, M=mean, SD=standard deviation.

In all, Thtot values of the Tp1-P inclusions cover a wide range from 230 to 460 °C, but cluster at 260 to 360 °C, and they show a decrease of Thtot from Tp1-P-G to Tp1-P-3s inclusions (Figure 16). Bulk densities of the Tp1-P inclusions range from 0.66 to 1.01 g/cm^3 with averages between 0.87 and 0.92 g/cm^3 (Table 2).

Tp1-S inclusions have XCO_2 values of 0.06 to 0.16 with a mean of 0.09 (Table 2). $TmCO_2$ values span a narrow range from -58.7 to -57.8 °C (Figure 14F). $ThCO_2(L)$ is between 21.8 and 28.4 °C (Figure 15F). Tmclat values range from 7.3 to 8.2 °C and Th(L) is between 245 and 338 °C (Figure 16F). Bulk salinities range from 3.7 to 5.2 wt% NaCl equivalent (Figure 22). CO_2 densities of the inclusions range from 0.65 to 0.75 g/cm^3 with an average of 0.71 g/cm^3 and bulk densities are from 0.87 to 0.97 g/cm^3 with an average of 0.94 g/cm^3. XCH_4 spans a range from 0.003 to 0.012, with an average of 0.007 (Table 2).

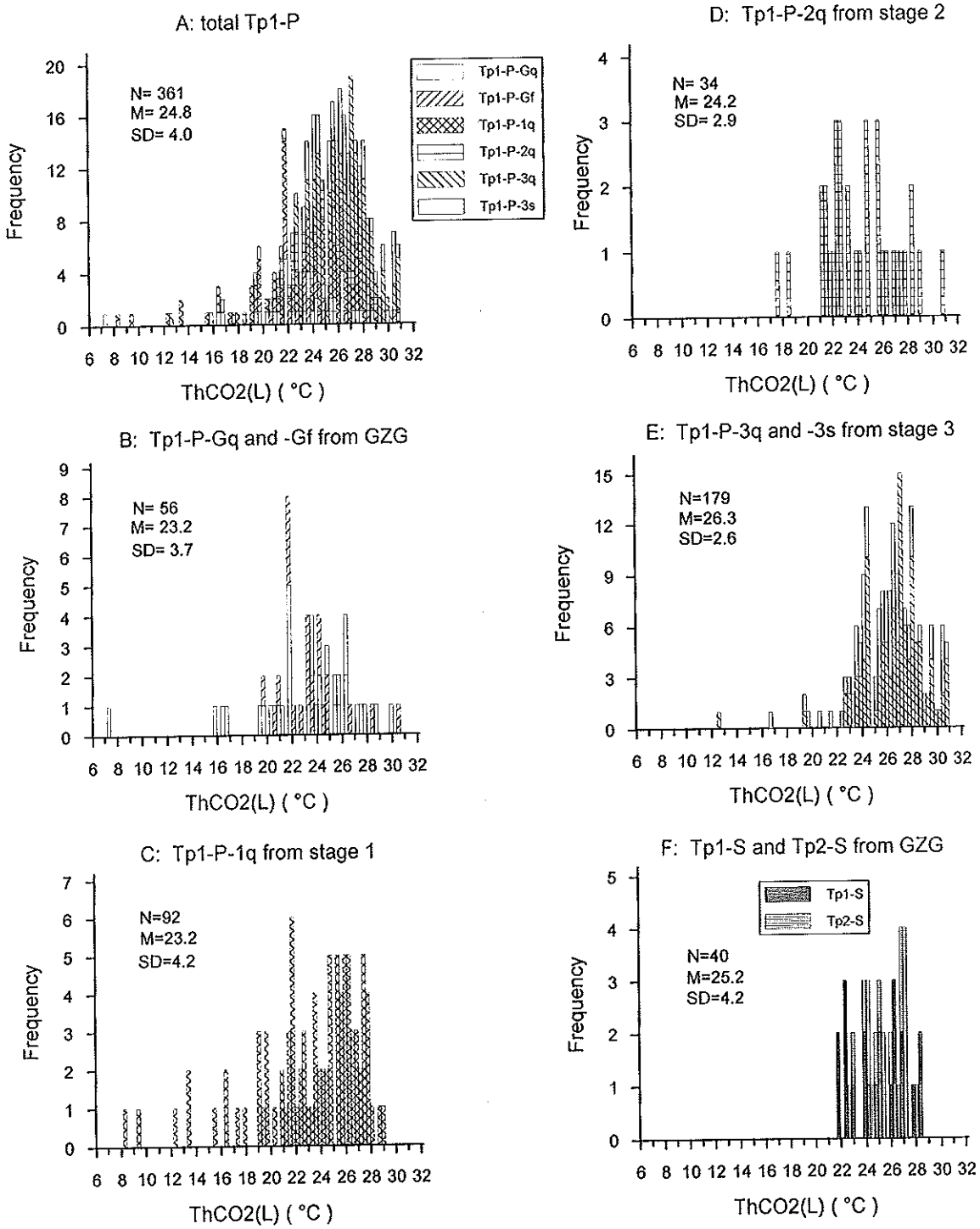

Figure 15. Frequency-$ThCO_2(L)$ histograms from fluid inclusion microthermometric data. $Th_{CO2}(L)$=homogenization temperature of carbonic phases into carbonic liquid. Abbreviations as in Figure 14.

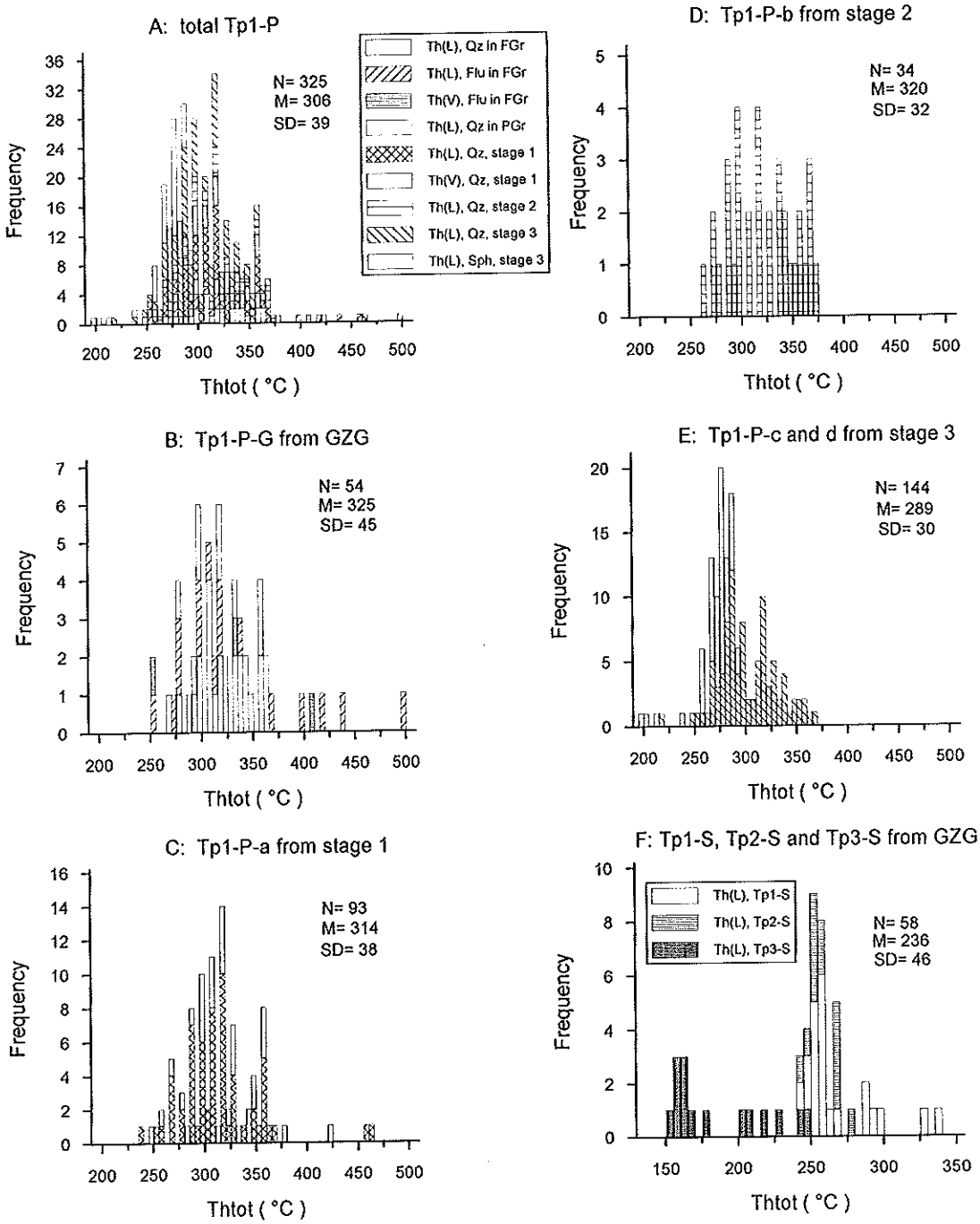

Figure 16. Frequency-Thtot histograms from fluid inclusion microthermometric data. Thtot=total homogenization temperature of fluid inclusions. Abbreviations as in Figure 14.

Tp2-S inclusions have XCO_2 values of 0.03 to 0.11 with a mean of 0.07 (Table 2). They are microthermometrically similar to those of the Tp1-S inclusions (Table 2). $TmCO_2$ values range from -58.6 to -57.9 °C (Figure 14F). $ThCO_2(L)$ values are between 23 and 27 °C (Figure 15F). Tmclat values range from 7.3 to 8.4 °C and Th(L) values span a range from 141 to 247 °C (Figure 16F). The solid phase does not melt at the range of total homogenization temperatures and its final dissolution temperatures were not determined. Bulk salinities of the inclusions range from 3.2 to 5.0 wt% NaCl equivalent (Figure 22). Average CO_2 and bulk

densities of the inclusions are 0.70 and 0.95 g/cm^3 (Table 2), respectively. XCH_4 averages 0.005 (Table 2).

Tp3-S inclusions have no detectable CO_2. Measurement of eutectic temperatures (Te) ranges from -27.9 to -17.6 °C with a mean of -23.4 ± 3.5 °C (1σ, n=17), which suggests that NaCl and KCl are the dominant solutes in the aqueous fluids (NaCl eutectic at -20.8°C, KCl eutectic at -10.6 °C, NaCl+KCl eutectic at -22.9 °C, Diamond, 1990). Final melting points of ice (Tmice) in the inclusions are between -3.5 and -1.4 °C with a mean of -2.5 ± 0.6 °C (1σ, n=17). Salinities estimated from the Tm_{ice} values range from 2.3 to 5.6 with an average of 4.1 ± 1.0 wt% NaCl equivalent (1σ, n=17) and Th(L) values are between 141 and 247 °C with a mean of 180 ± 34 °C (1σ, n=18) (Figure 16F, Table 2).

STABLE ISOTOPES

Carbon Isotopes

Table 3 shows analytical results of carbon, oxygen and hydrogen isotope compositions of selected hydrothermal minerals and fluid inclusions. $\delta^{13}C$ values of carbonates from stage 4 are between -6.3 and -2.5‰ (mean -4.4‰, n=5), which are consistent with those of fluid inclusion CO_2 in vein quartz from stages 1 to 3, with $\delta^{13}C$ values of -6.1 to -4.3‰ (mean -5.2‰, n=7, Figure 17).

As shown in Figure 18, the $\delta^{13}C$ values of fluid inclusion CO_2 in vein quartz show a decreasing trend of about 0.5 to 1‰ from stages 1 to 2 and an increasing trend of about 1 to 1.5 ‰ from stages 2 to 3. The former may be related to a mixing process of the ore-forming fluids with external fluids, while the latter may mainly reflect the effect of temperature on

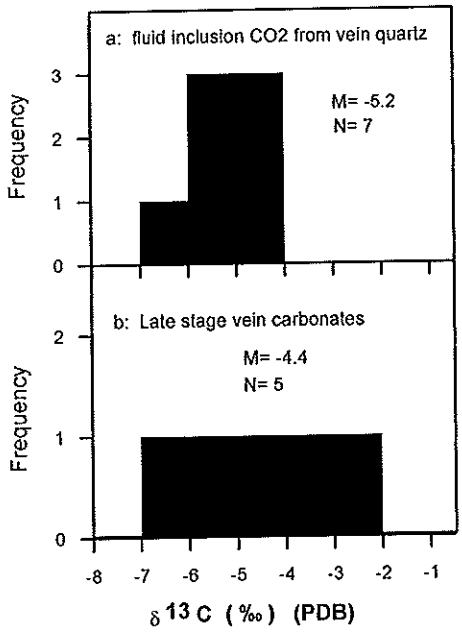

Figure 17. Histogram of $\delta^{13}C$ values for fluid inclusion CO_2 in vein quartz from stages 1 to 3 and for vein carbonates from stage 4 in the Niuxinshan gold deposit.

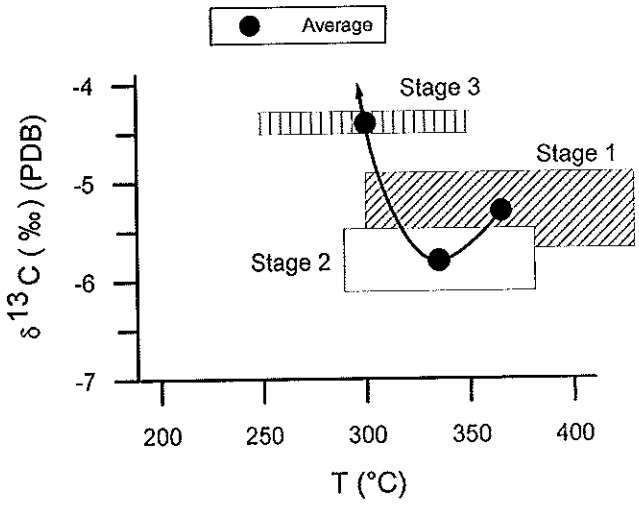

Figure 18. Diagram of carbon isotope compositons for fluid inclusion CO_2 in vein quartz from stages 1 to 3 in the Niuxinshan gold deposit. Temperatures based on isochores of fluid inclusions.

Table 3. Carbon, oxygen and hydrogen isotope data for hydrothermal minerals and fluid inclusions from the Niuxinshan gold deposit (after Yao, 1997)

Sample	T* (°C)	Type	Host rock	Mineral	δ^{18}Omin ‰ (SMOW)	δ^{18}Ofi ‰ (SMOW)	δDmin ‰ (SMOW)	δDfi ‰ (SMOW)	δ^{13}Cmin ‰ (PDB)	δ^{13}Cfi ‰ (PDB)	Tfi °C	Tqz-mus/ qz-Kf °C	Ref.
6035		LGr	Gr	Qz	11.2								1
6139		LGr	Gr	Qz	10.6								1
6177		LGr	Gr	Qz	10.8								
6035		LGr	Gr	Kf	11.2								1
6139		LGr	Gr	Kf	12.9								1
6177		LGr	Gr	Kf	11.6								1
6140		WGr	Gr	Ser	9.3							659	1
6141		WGr	Gr	Ser	8.7							688	1
6143		FGr	Gr	Qz	12.3	6.6					335	328	1
6143		FGr	Gr	Ser	8.4		-45	-20			335		
6145		FGr	Gr	Qz	12.7	6.8					328	328	1
6145		FGr	Gr	Ser	8.8		-48	-23			328		
6041		FGr	Gr	Qz	13.1	7.2					328		1
6041		FGr	Gr	Ser	11.5						328		
6038		PGr	Gr	Qz	12.3	5.9					313		1
6038		PGr	Gr	Ser	10.9		-51	-26			313		
6133		PGr	Gr	Qz	13.1	6.7					313	460	1
6133		PGr	Gr	Ser	10.5		-50	-25			313		1
6181	100-310	VS 1	Amp	Qz	11.6	5.2		-70		-5.7	314		1, 2
6181	310-415	VS 1	Amp	Qz				-72			314	493	1
6181		VS 1	Amp	Kf	10.0						314		
6020	100-400	VS 1	Amp	Qz	10.9	4.5		-69		-4.9	314	470	1, 2
6020		VS 1	Amp	Kf	9.2						314		
6111		VS 1	Amp	Qz	10.6	4.2					314	430	2
6111		VS 1	Amp	Kf	8.7						314		
6555		VS 1	Amp	Qz	11.7	5.3					314	1098	2
6555		VS 1	Amp	Kf	11.2						314		
6021	100-350	VS 2	Amp	Qz	12.9	6.4		-68		-6.1	310		1
6021	350-480	VS 2	Amp	Qz				-69			310		1
6021	480-550	VS 2	Amp	Qz				-80			310		1
6121	100-350	VS 2	Amp	Qz	14.0	7.1		-70		-5.5	300		1
6018	100-300	VS 3	Amp	Qz	11.2	3.9		-68		-4.3	289		1
6018	300-500	VS 3	Amp	Qz				-71			289		1
6119	100-310	VS 3	Amp	Qz	12.8	5.9		-77		-4.5	300		1
6119	310-450	VS 3	Amp	Qz				-73			300		1
21		VS 3	Amp	Qz	13.0	6.8		-86			319		3
50		VS 3	Amp	Qz	12.1	5.5					306		3
CE89059		VS 3	Amp	Qz	13.3	6.7		-64		-5.4	307		3
6118		VS 4	Amp	Ank	15.8				-2.5				1
6147		VS 4	Amp	Cal	12.8				-4.7				1
6191		VS 4	Amp	Ank	10.6				-3.3				1
6605		VS 4	Amp	Ank	10.4				-5.4				1
6173		VS 4	Amp	Dol	9.7				-6.3				2

Summary	N	Min	Max	M	SD	
δ^{13}Ccarb	5	-6.3	-2.5	-4.4	1.4	
δ^{13}Cfi	7	-6.1	-4.3	-5.2	0.6	
δ^{18}Ocarb	5	9.7	15.8	11.9	2.2	
δ^{18}Oqz, vein	11	10.6	14	12.2	1.0	
δ^{18}Oser	7	8.4	11.5	9.7	1.1	
δ^{18}Okf, vein	4	8.7	11.2	9.8	0.9	
δ^{18}Ofi, qz	11	3.9	7.1	5.6	1.0	
δDfi, qz	13	-86	-64	-72	5.5	
δDfi, ser	4	-26	-20	-24	2.3	
δDser	4	-51	-45	-49	2.3	
δDH2O, ser	4	-20	-20	-24	2.3	
Niuxinshan granitoids						
δ^{18}Oqz	3	10.6	11.2	10.9	0.2	
δ^{18}OKf	3	11.2	12.9	11.9	0.7	
Regional granitoids						3, 4
δ^{18}Oqz, Gr	4	5.3	10.3	7.8	2.4	
$\delta^{18}OH_2O$, Gr	4	7.8	9.3	8.6	0.7	
δDH_2O, Gr	4	-92	-72	-79	8	

Note: min=mineral, Kf=K-feldspar, Ser=sericite, Mus=muscovite, Qz=quartz, Carb=carbonates, Cal=calcite, Ank=ankerite, Dol=dolomite, fi=fluid inclusion. WGr=weakly altered granite, Gr=granite, Amp=amphibolites. FGr=greisenization with fluorite, PGr=greisenization with pyrite. VS1=stage 1 of quartz-K-feldspar vein, VS 2=stage 2 of quartz-pyrite vein, VS 3=stage 3 of quartz-polysulfide vein, VS 4=stage 4 of quartz-carbonate vein. T*: extraction temperatures of fluid inclusions from vein quartz. Tfi: temperatures from average fluid inclusion microthermometry. Tqz-mus/qz-Kf: temperatures estimated from oxygen isotope fractionation factors of quartz-muscovite (Chacko et al., 1996) and quartz-K-feldspar pairs (Trumbull et al., 1992), respectively. δ^{18}Ofi: calculated from fractionation factors of oxygen isotopes between quartz-water (Matsuhisa et al., 1979). δDH_2O: calculated from fractionation factors of hydrogen isotopes between sericite-water pairs (Sheppard and Gilg, 1996). Ref.: 1=this study, 2=Trumbull et al. (1992), 3= Bai et al. (1990), 4=Zhang et al. (1991).

carbon isotope fractionation (Ohmoto and Rye, 1979). However, more carbon isotope analyses of fluid inclusion CO_2 in vein quartz from each stage are needed to trace the trend of carbon isotopes through time. Assuming that the average $\delta^{13}C$ values of fluid inclusions (-5.2‰) represents the carbon isotope compositions of CO_2 in equilibrium with the carbonates, the carbon isotope fractionation between CO_2 and carbonates (Bottinga, 1968) indicates temperatures of 108 to 226°C with a mean of 160 °C for the formation of carbonates. The 226 °C is compared with the temperature 240 °C estimated by chlorite geothermometry from the sericite-chlorite-carbonate zone in the amphibolites (Bai et al., 1990). This suggests that the vein carbonates were formed at lower temperatures (e.g. stage 4), as indicated by the mineral paragenesis.

Oxygen Isotopes

Oxygen isotope compositions of quartz and K-feldspar in the least-altered granite are presented in the section of Niuxinshan granite. Quartz and sericite (muscovite) from the altered granite display $\delta^{18}O$ values between 10.2 and 13.1‰ (mean 12.1‰, n=7), and 8.4 and 11.5‰ (mean 9.7‰, n=7), respectively. The quartz is enriched in $\delta^{18}O$ relative to the coexisting sericite in each sample and shows a trend of decreasing $\delta^{18}O$ values with alteration toward the granite (Yao, 1997). This indicates an oxygen isotope equilibrium between quartz and sericite (Chacko et al., 1996). The oxygen isotope equilibrium temperatures, using the fractionation factors between quartz and sericite of Chacko et al. (1996), were estimated to be between 328 and 720 °C from 5 samples (Table 2). Two samples give temperatures at 660 and 720°C, which are geologically unreasonable, whereas the other three samples give temperatures at 328, 328 and 460°C, which are consistent with the fluid inclusion microthermometric data from the alteration zones. The two highest temperatures may result from oxygen isotope modifications at a later stage during infiltration and diffusion processes of alteration.The$\delta^{18}O$

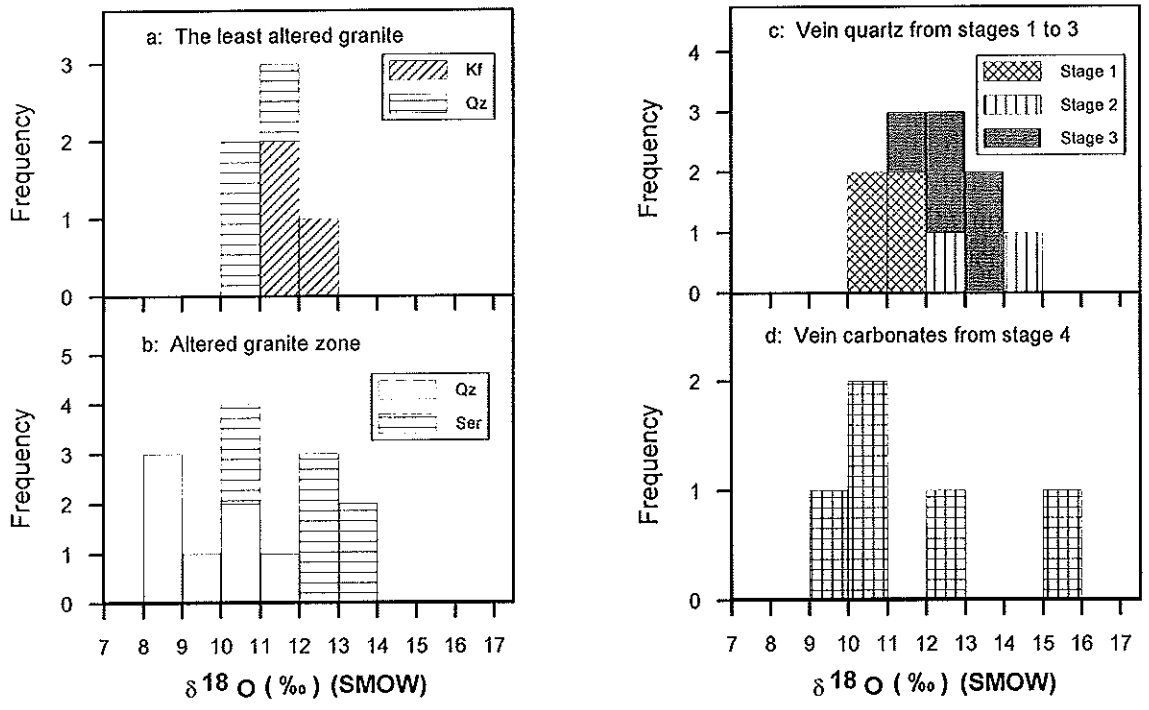

Figure 19. Histograms of oxygen isotopic compositions for quartz and K-feldspar from the least-altered granite, for quartz and sericite from the altered granite zone and for vein quartz from stages 1 to 3 and vein carbonates from late stage 4.

The $\delta^{12}O$ values of water, calculated from the $\delta^{18}O$ values of quartz in the alteration zone, using the fractionation factors of Matsuhisa et al. (1979) at temperatures of 313 to 328 °C from the average fluid inclusion microthermometry, range from 4.2 to 7.2‰ (mean 6.0‰, n=7).

$\delta^{18}O$ values of vein quartz from stages 1 to 3 range from 10.6 to 14.0‰ with a mean of 12.2±1.0‰ (n=11). The calculated $\delta^{18}O$ values of water (Matsuhisa et al., 1979) at temperatures of 298 to 314°C from the average fluid influsion microthermometry cluster at 3.9 and 7.1‰ (mean 5.6 ± 1.0‰, n=11). The $\delta^{18}O$ values of vein quartz increase by about 2‰ from stage 1 to stage 2, but decrease by about 1‰ from stage 2 to stage 3 (Yao, 1997). This suggests that the oxygen isotope compositions of ore-bearing fluids decreased due to addition of meteoric waters. Since the oxygen isotope fractionation factors between quartz and water increase with decreasing temperature (Matsuhisa et al. 1979), the $\delta^{18}O$ values of quartz at equilibrium with a uniform fluid will increase at lower temperature, and this is not observed.

$\delta^{18}O$ values of K-feldspar in stage 1 range from 8.7 to 11.2‰ with a mean of 9.8‰ (n=4), which are lower than those of coexisting quartz in each sample (Table 2). The estimated oxygen isotope equilibrium temperatures between quartz and K-feldspar in stage 1 are between 430 and 493°C (Trumbull et al., 1992). The $\delta^{18}O$ values of late stage 4 vein carbonates range from 9.7 to 15.8‰ (mean 11.9‰, n=5). In general, these oxygen isotope compositions of vein quartz, muscovite, K-feldspar and carbonates from different stages span a range from 8 to 16‰, and commonly cluster at 10 to 13‰ (Figure 19).

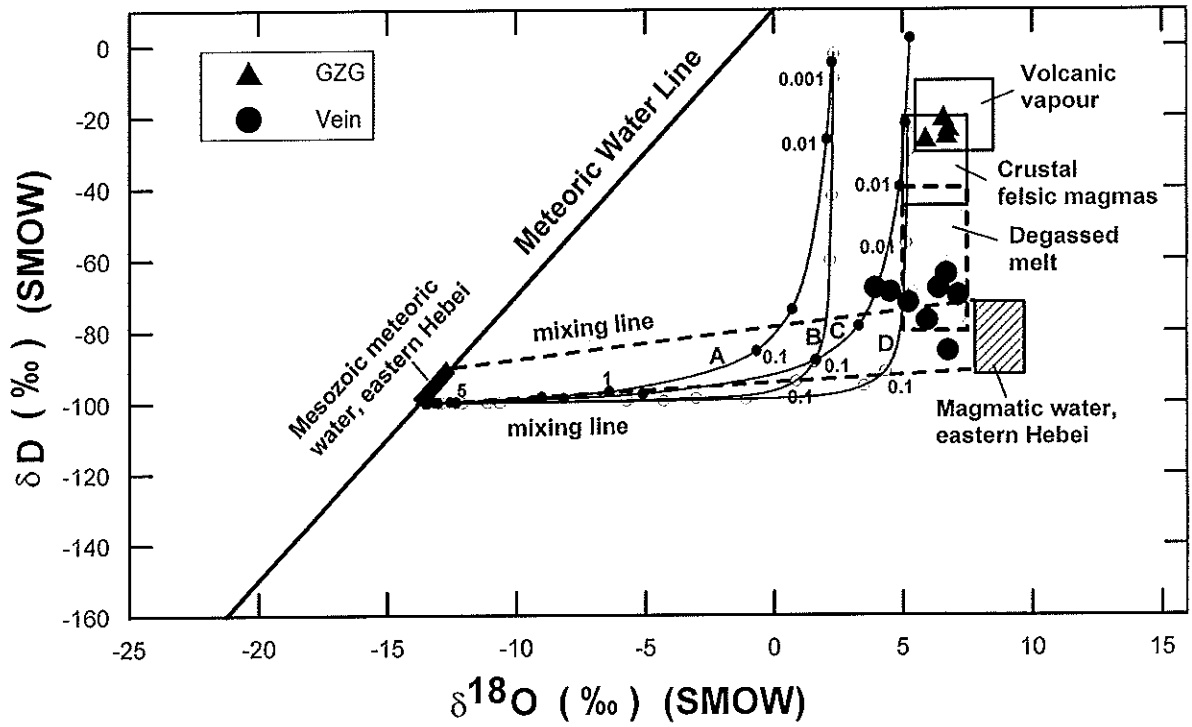

Figure 20. Diagram of oxygen and hydrogen isotope compositions of ore-bearing fluids and evolved Mesozoic meteoric waters in equilibrium with amphibolites and granites from the Niuxinshan gold deposit. Also shown are oxygen and hydrogen isotope fields of volcanic vapour, crustal felsic magmas, degassed melt (Hedenquist and Lowenstern, 1994) and magmatic waters in eatern Hebei Province (Bai et al., 1990; Zhang et al., 1991). Curves A and C represent isotopic evolution of meteoric water in equilibrium with the regional metamorphic rocks at temperatures of 250 to 350 °C, whereas curves B and D represent isotopic evolution of meteoric water in equilibrium with the regional granitoids at temperatures of 250 to 350 °C. GZG=greisen zone in the granite.

Hydrogen Isotopes

Hydrogen isotope compositions of sericite in the altered granite zone span a narrow range from -51 to -45‰ (mean -48.5‰, n=4), the δD values of water estimated from fractionation factors between sericite and water (Sheppard and Gilg, 1996) at 350 ± 50 °C are betweeen -26 and -20‰ (mean -23.5‰, n=4), which are consistent with hydrogen isotope compositions of volcanic gases (-10 to -30‰, Hedenquist and Lowenstern, 1994). Measured δD values of fluid inclusions in vein quartz from stages 1 to 3 fall in a range from -85 to -64‰ (mean -71‰, n=8). δD values of Mesozoic magmatic waters from eastern Hebei, estimated from biotite (-104‰) and hornblende (-90‰) and measured from fluid inclusions in quartz from granites, are between -72 and -92‰ with a mean of -79‰ (Table 3, n=4), which are compatible with those of fluid inclusions from vein quartz in the Niuxinshan gold deposit.

The δD and $\delta^{18}O$ values of fluids at Niuxinshan overlap the isotopic fields of degassed volcanic vapour and melt (Figure 20), which indicates that the ore-bearing fluids were magmatic hydrothermal fluids. As pointed out by Taylor (1986), depletion of δD (commonly -40 to -80‰) in magmatic fluids is caused by magma degassing at a late stage.

Sulphur Isotopes

Isotope compositions of sulphur in pyrite, sphalerite and galena in the Niuxinshan gold deposit span a narrow range from 2.8 to 6.3‰ with a mean of 5.4‰ (Figure 21) and are enriched in the order of pyrite-sphalerite-galena (Bai et al., 1990), indicating isotopic equilibrium of sulphur in the fluids depositing sulphides (Ohmoto and Rye, 1979). The $\delta^{34}S$ values in pyrite from vein quartz in the Archaean amphibolites are quite similar to those from the greisen ores in the granite, which suggests that both of the ore sulphides were formed by the ore-bearing fluids with homogeneous sulphur isotope compositions (Yao, 1997).

The sulphur isotope fractionation between sphalerite and galena gives a temperature of 381 °C for sulphide formation (Bai et al., 1990). Based on mineral paragenesis and sulphide abundance of ores, total sulphur isotope compositions of the ore-bearing fluids were estimated to be about 5.4‰ (Bai et al., 1990). This is comparable with the sulphur isotope compositions of magmatic fluids (e.g. Ohmoto and Rye, 1979).

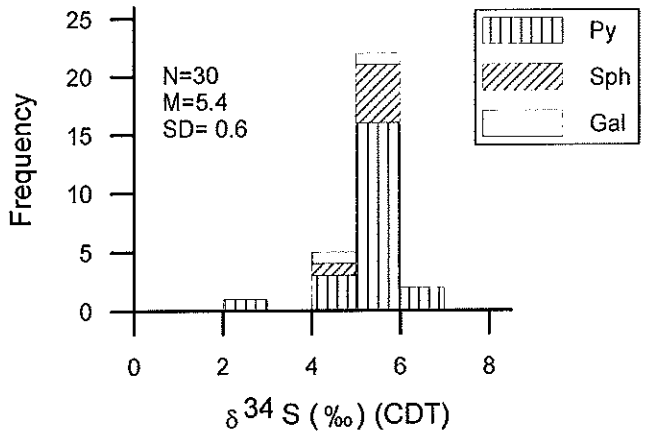

Figure 21. Histogram of sulphur isotopic compositions for sulphides from the Niuxinshan gold deposit. Py=pyrite, Sph=sphalerite, Gal=galena. N=sample number, M=mean, SD=standard deviation. Data are from Bai et al. (1990).

DISCUSSION

P-T Conditions of Trapped Fluids

Pressure-temperature conditions of trapped fluids at Niuxinshan were constructed from the microthermometric data of fluid inclusions, in combination with mineral phase equilibria, isotope geothermometry and geological evidence. The isochores of all the fluid inclusion types are plotted in Figure 22 (Yao, 1997; Yao et al., 1999).

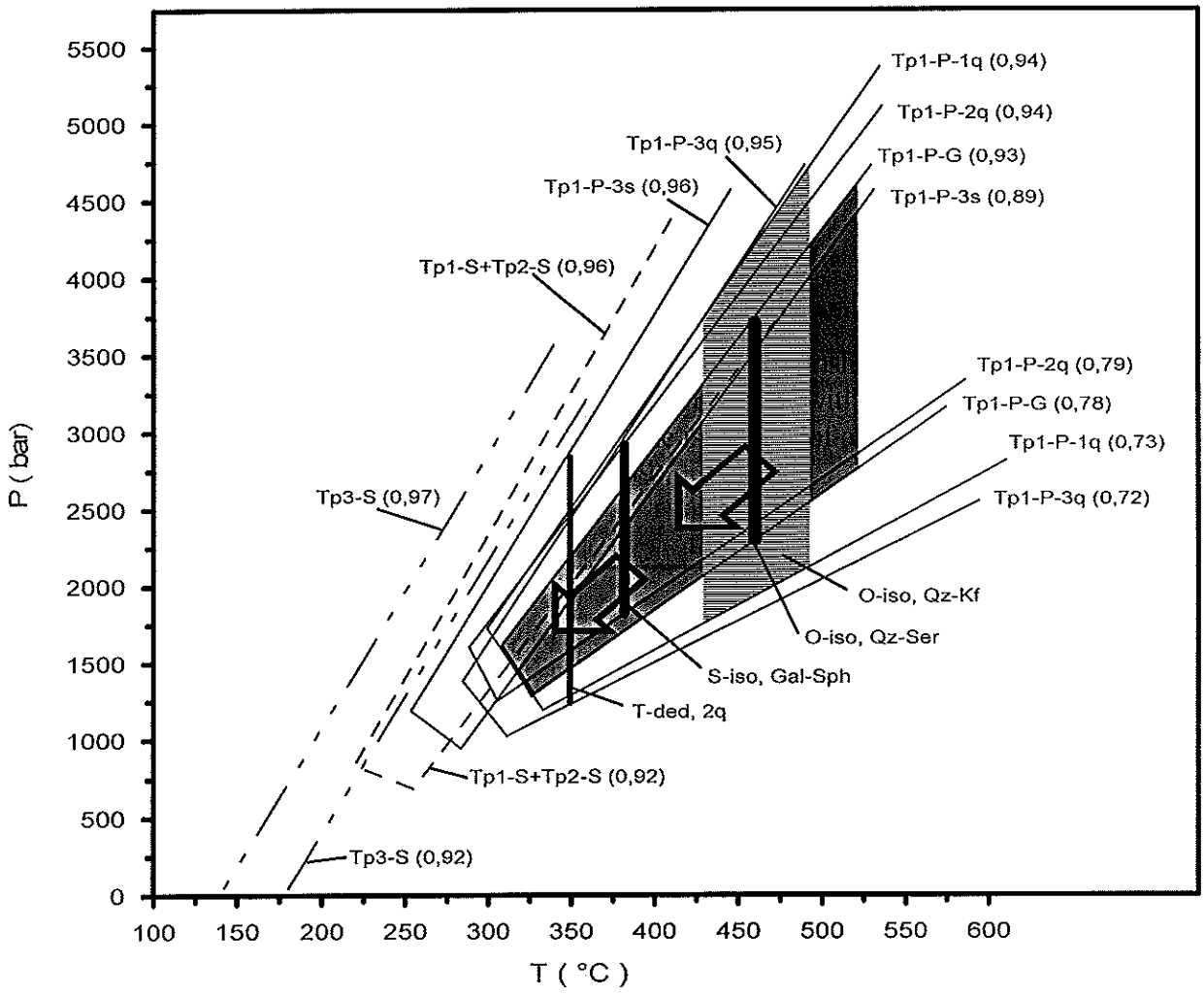

Figure 22. Pressure-temperature evolution reconstructed from isochores of primary (Tp1-P) and secondary (Tp1-S, Tp2-S and Tp3-S) fluid inclusions. The dark-shaded field represents the P-T space of isochores for the Tp1-P-G fluid inclusions from greisen zones in the granite. The ruled area indicates upper temperature limits of 439 to 493 °C for the Tp1-P-1q in stage 1 from oxygen isotope equilibrium temperatures of quartz and K-feldspar pairs (O-iso, Qz-Kf) after Trumbull et al. (1992). The dark vertical bars represents temperature limits from stable isotope thermometry: 460 °C from oxygen isotopes of quartz and sericite from greisen zones in granite (O-iso, Qz-Ser) after Yao (1997), and 381 °C from sulphur isotopes of galena and sphalerite pairs (S-iso, Gal-Sph) after Bai et al. (1990). The fine vertical line represents the upper temperature limit of 350 °C for the Tp1-P-3q and -3s in stage 3, deduced from the upper pressure at 3 kbar from the Tp1-P-2q (T-ded, 2q). Also shown are bulk densities (g/cm^3) of all the fluid inclusion isochores in parentheses. Abbreviations as in Figure 14. From Yao et al.(1999).

The isochores of Tp1-P-G inclusions define the trapped P-T at 310 to 460 °C and 1.3 to 3.7 kbar for the greisen zones. Stage 1, represented by the Tp1-P-1q inclusion isochores, formed at 300 to 430 °C and 1.2 to 3.7 kbar; stage 2 at 290 to 380 °C and 1.3 to 3 kbar; Stage 3 at 250 to 350 °C and 1 to 3 kbar. The isochores of Tp1-S+Tp2-S inclusions define the minimum trapping temperature and pressure at about 220 to 250 °C and 0.7 to 0.8 kbar; and the isochores of Tp3-S inclusions define the minimum temperature and pressure at about 140 to 180 °C and 4 to 15 bar.

Figure 22 also shows a possible evolutionary path that fits the P-T constraints for the ore-forming fluids at Niuxinshan. The retrograde P-T path drops successively through isochores of primary Tp1-P-G, Tp1-P-1q, -2q, -3q, and Tp1-P-3s to secondary Tp1-S, -2-S, and Tp3-S. The temperatures of formation for greisenization and vein stages 1 to 3 are constrained by independent isotope equilibrium geothermometry and by fluid inclusion microthermometry, which are generally consistent with temperature estimates from the mineral assemblages. Cooling of the fluids during multistage mineralization is also reflected by cross-cutting relationship between early and late stage veins with various mineral parageneses. It must be noted, however, that the pressures during mineralization are not well constrained. Indications for a pressures decrease with time from the inclusion data are based on the decreasing temperature and isochore intersections, and are likely to have resulted from regional uplift and cooling of vein-forming hydrothermal fluids (Bai et al., 1990; Zhang et al., 1991). Repeated fracturing, as inferred from the local geology, may have caused pulsed evolution of the hydrothermal fluids, with some fluctuations in fluid pressure (Yao et al., 1999).

Source of Ore-Forming Fluids

The ore-forming fluids at Niuxinshan are H_2O-CO_2-bearing solutions, with low to moderate salinities (commonly 3 - 11 wt% NaCl equivalent) and CO_2 contents (mainly 10 - 40 mole %), and were trapped at 250 to 380 °C and 1 to 3 kbar for the main gold mineralization from stages 2 to 3 (see above). The fluids are similar to those of most mesothermal gold deposits in eastern Hebei Province (Yu and Jia, 1989; Bai et al., 1990; Zhang et al., 1991; Trumbull et al., 1992) and of similar deposits in Korea (Shelton et al., 1988; So et al., 1995). They are also comparable with those of mesothermal lode gold deposits in the Archaean greenstone terranes worldwide, except for the lower salinities (typically <5 wt% NaCl equivalent) in the latter (see Ho, 1987; Groves and Forster, 1991; De Ronde et al., 1992; McCauig and Kerrich, 1994; Solomon and Groves, 1994).

It has been suggested that the fluid source in many of the Archaean mesothermal gold deposits is metamorphic (cf. Groves and Forster, 1991; McCauig and Kerrich, 1994; Solomon and Groves, 1994). However, magmatic sources have also been proposed by Burrows et al. (1986), Burrows and Spooner (1987), Hattori (1987), and Spooner (1991). Additionally, Nesbitt and Muehlenbachs (1989) proposed that mesothermal lode gold deposits in the Canadian Cordillera were generated by evolved meteoric waters, and Witt et al. (1997) suggested that synmetamorphic hydrothermal fluids were responsible for the formation of gold deposits in the Archaean South Kalgoorlie and Norseman terranes, Western Australia.

Regional metamorphic fluids are not a viable source for the mineralization at Niuxinshan because the Mesozoic age of mineralization at the deposit is about 2000 Ma later than the age of metamorphism in the basement rocks (Trumbull et al., 1992). Instead, the source of the ore-forming fluids at Niuxinshan is considered to be mainly magmatic fluids, with partial mixing of meteoric waters (Yao, 1997). This is based on the character of the fluid inclusions and the stable isotopes of gangue minerals, in combination with the ore geology and geochemistry.

The $\delta^{18}O$ and δD values of waters (Figure 20), estimated from oxygen and hydrogen isotopes of vein quartz, alteration sericite, and fluid inclusions in vein quartz, coincide with those of magmatic fluids (Taylor, 1986; Hedenquist and Lowenstern, 1994). They are comparable to those from the Jungwon Mesozoic gold deposits of Korea (So et al., 1995) and the Mink Lake Mo-Au-W showing in Canada (Burrows and Spooner, 1987), which were regarded as being of magmatic origin. However, they differ from the fluids of the Archaean lode gold deposits, which are thought to be derived from metamorphic waters (e.g. Groves and Foster, 1991), and from the fluids in the mesothermal gold deposits of the Canadian Cordillera, modelled as meteoric waters by Nesbitt and Muehlenbachs (1989).

Although the quartz veins clearly post-date the emplacement of the Niuxinshan granite, mafic and felsic dykes are coeval with the quartz veins, indicating that magmatism was still active at the time of mineralization. The carbon and sulphur isotope compositions of carbonates, fluid inclusion CO_2 and sulphides are also consistent with a magmatic origin of the carbon and sulphur at Niuxinshan, but they cannot rule out the possibility of average crustal carbon and sulphur. However, it must be noted that the source of the fluids is not necessarily the same as the source of the carbon and sulphur.

In order to assess the importance of meteoric waters in the Niuxinshan gold deposit, the oxygen and hydrogen isotope compositions of meteoric waters in equilibrium with the regional metamorphic rocks and granitoids were estimated using the methods of Taylor (1977) and Criss and Taylor (1986). Figure 20 shows the isotopic evolution of meteoric waters in equilibrium with both wall rocks at a given temperature. At 250°C, the evolved meteoric waters could not generate the isotopic compositons of the ore fluids. However, at 350°C, some data points are near the C and D curves at very low water/rock ratios (0.05 to 0.005). In addition, some isotopic compositions may have been generated by direct mixing of meteoric waters with the ore-bearing fluids (Figure 20). This suggests some contribution of meteoric waters to the mineralizing fluids, which is also supported by the relationship between the bulk salinities and total homogenization temperatures of the fluid inclusions studied (Yao et al., 1999).

The dominantly magmatic-derived fluids at Niuxinshan are similar to those described by Nabelek and Ternes (1997) in a fluid inclusion study of the Harney Peak Granite, Black Hills, South Dakota. These authors identified primary magmatic-exsolved H_2O-CO_2 fluids with salinites of 1 to 10 wt% NaCl equivalent and could trace their evolution from CO_2-rich towards saline H_2O-rich compositions during progressive crystallization of the granite. The low saline (<10 wt% NaCl equivalent) H_2O-CO_2 fluids from As-Sb-Au veins in Newfoundland (Kay and Strong, 1983) and in the Mo-Au-W mineralization in Mink Lake, northwestern Ontario (Burrows and Spooner, 1987) have also been considered to be magmatic fluids.

Gold Deposition

The similarity of microthermometric data for the Tp1-P, Tp1-S and Tp2-S inclusions suggests that the trapped fluids had similar compositions throughout the mineralization sequence. Because some gold occurs along microcracks within quartz and sulphides (mainly pyrite), it is possible that the secondary Tp1-S, Tp2-S, and Tp3-S inclusions may also have trapped gold-bearing fluids.

The main gold species in mesothermal hydrothermal fluids are believed to be gold dichloride and/or thio complexes (Henley, 1973; Seward, 1973, 1984b, 1991), whose solubilities are generally expressed as follows (Seward, 1984b):

$Au^\circ + H_2S\ (aq) + HS^- = Au(HS)_2^- + 0.5\ H_2\ (g)$ (1)

$Au^\circ + 2H^+ + 2Cl^- = AuCl_2^- + H_2\ (g)$ (2).

The thio complex of gold dominates under reducing conditions at near-neutral pH values and at relatively low temperatures (Seward, 1984b, 1991). The abundance of base-metals (Cu, Pb, Zn) in the ores at Niuxinshan suggests the presence of chloride-metal complexes in the ore fluids (Barnes, 1979; Seward, 1984a). However, this does not necessarily mean that gold was also transported as a chloride complex. Yao (1997) calculated gold solubilities as thio and dichloride complexes using equilibrium constants from equations 1 and 2, the P-T-X data of fluid inclusions, and compositional parameters calculated from salinities of inclusions (aCl^-, ionic activities), mineral assemblages (pH, f_{S2}), and equilibrium relations in the C-H-O-S system, including CO_2-CH_4 (fO_2), H_2-O_2 (fH_2), H_2S-O_2 (aH_2S), and H^+-HS^- (aHS^-) (Yao, 1997, and references therein). The pH of the fluids, based on the stable coexistence of K-feldspar and sericite in proximal vein selvages, is between 5 and 6, which is consistent with the estimates of Mikucki and Ridley (1993), and Cassidy and Bennett (1993) for other mesothermal gold deposits. The lack of argillic alteration also indicates that fluids were not acidic (Cassidy and Bennett, 1993) at the mineralization temperature. The fO_2 values were estimated by the CH_4-CO_2 equilibrium to be between 10^{-24} and 10^{-38} at 460 to 250 °C, respectively. This gives lower limits of the fO_2 for the ore-forming fluids (Mikucki and Ridley, 1993). The lack of sulphate minerals at Niuxinshan, and the indications for CH_4 in the inclusions, suggest that the fluids were reduced. This is consistent with the above estimated fO_2 values which are below the field of hematite in equilibrium with pyrite (Yao, 1997).

Based on these thermodynamic calculations (Yao, 1997; Yao et al., 1999), Au $(HS)_2^-$ solubilities range from about 30 to 12000 ppb for conditions in the greisen zones, from 12 to 150 ppb for stage 2 conditions, and from 0.2 to 89 ppb for stage 3. Under the same conditions the $AuCl_2^-$ solubilities are about four orders of magnitude less, from $1.4*10^{-4}$ to 1 ppb for the greisen zone conditions, from $3*10^{-5}$ to $9*10^{-3}$ ppb for stage 2, and from $7.6*10^{-7}$ to $1.3*10^{-3}$ ppb for stage 3. It is suggested, therefore, that gold was transported as the $Au(HS)_2^-$ complex in the ore-forming fluids. Gold deposition at Niuxinshan would mainly depend on the decrease of temperature and pressure, and on sulphidization of wall rocks, which lowers the hydrosulphide activity and destabilizes the Au $(HS)_2^-$ complex (equation 1).

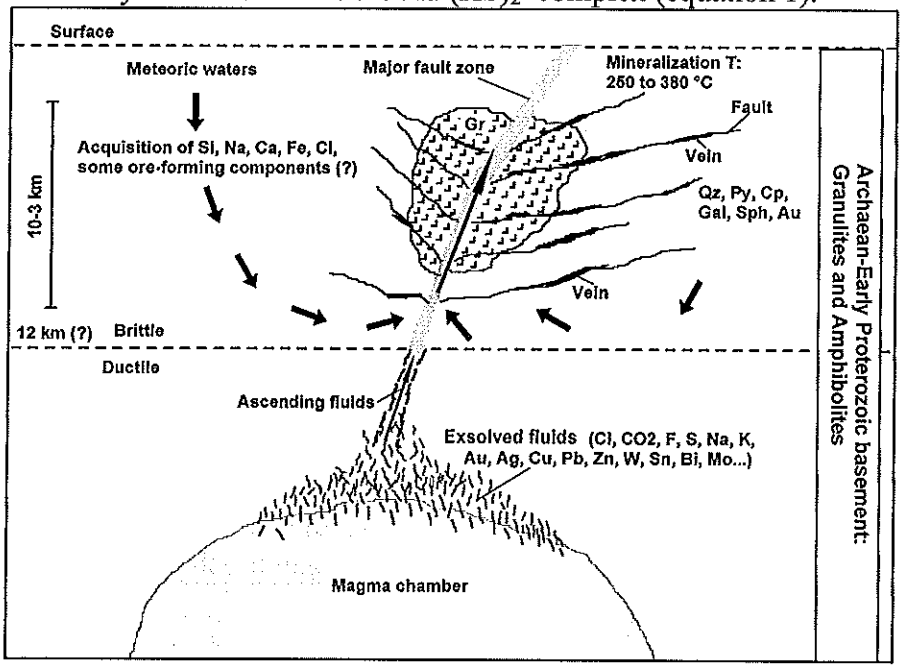

Figure 23 Schematic diagram of a genetic model showing the movement of degassing magmatic hydrothermal fluids and the mixing of partial meteoric waters in the brittle deformation regime for the Niuxinshan gold deposit. Gr=Niuxinshan granite. For interpretation see text.

Genetic Model

On the basis of the geology, geochemistry, fluid inclusions, and stable isotopes of gold ores in the Niuxinshan deposit, a genetic model of degassing magmatic hydrothermal fluids with partial mixing of meteoric waters is proposed and shown schematically in Figure 23. The model stresses the following processes:

(1) the Niuxinshan granite emplacement: the granite intruded into the Archaean basement (Qianxi Group) at about 179 Ma during the Yanshanian period (Bai et al., 1990), at which the Sino-Korean platform was reactivated by faulting and magmatism;

(2) structural controls: the Yanshanian NE-NNE-striking faults and fractures control the granite emplacement and gold mineralization;

(3) magma chamber: it is speculated that an unexposed and active magma at depth may have provided the exsolved fluids and ore metals for the mineralization. This proposition is based on the following facts: (a) geological evidence indicates that the ore veins post-dated the granite, and this suggests that the Niuxinshan granite itself does not represent the source magma for the mineralization; (b) cross-cutting relationships between the dykes, (especially the lamprophyres) and veins (section 3) indicate the presence of magma at depth during and closely following the time of mineralization. At present, the lack of petrogenetic data for the dykes precludes further discussion on the nature of this late magmatism;

(4) the magmatic hydrothermal fluids: these fluids were derived by the exsolution of volatiles from the magma chamber at a late stage. The exsolved fluids contain ore-forming metals, and ascended along the major NE-NNE-striking fault zone from the lower to the upper crust. In the brittle regime, the fluids were partially mixed with meteoric waters. The meteoric waters may have brought additional components to the fluids by leaching the country rocks;

(5) the mixed fluids in the brittle settings reacted with the wall rocks to generate alteration zones along the borders of the quartz veins; and

(6) gold was transported mainly as a sulphide complex ($Au(HS)_2^-$) and deposited due to the cooling of the fluids and the sulphidization of the wall rocks at temperatures of 250 to 380 °C and pressures of 1 to 3 kbar.

CONCLUSIONS

1. The Niuxinshan gold quartz veins formed during the Yanshanian tectono-magmatic reactivation of the North China craton. The gold is related to the sulphides (mainly pyrite) in the quartz-pyrite stage 2 and quartz-polysulphide stage 3. The geochemical data and the Sr, O, and Pb isotope characteristics suggest that the Niuxinshan granite is an I-type granite, which was generated by the partial melting of infracrustal source materials.

2. The alteration is characterized by an inner greisenization±pyritization and an outer sericitization zone in the granite, and by an inner sericitization+silicification, and an outer chloritization+sericitization+ carbonatization zone in the amphibolites. In the vicinity of the granite, K-feldspathization and/or fluoritization occur locally. Mass balance calculations indicated that a large amount of Si and all of the Na were lost in both alteration zones. The ore-forming elements (Cu-Pb-Zn-Au-Ag-W-Sn-Bi-Mo) and volatile species (CO_2, S, F) were intensively added into the alteration haloes by the mineralizing fluids, whereas Ti, Al, Fe, Mg, and REE were locally buffered by the two host rocks.

3. Three types of fluid inclusions were recognized. Type 1 are primary (Tp1-P) and secondary (Tp1-S) H_2O-CO_2-NaCl inclusions; Type 2 are secondary H_2O-CO_2-NaCl+solid phase inclusions; and Type 3 are secondary H_2O-rich inclusions with a solid phase. The ore-

forming fluids are H_2O-CO_2 solutions with low to moderate salinities of mainly 3 to 11 wt% NaCl equivalent and XCO_2 values of commonly 0.1 and 0.4. The fluids evolved toward H_2O-rich and CO_2- and NaCl-poor compositions through time. The isochore-constrained PT conditions of mineralization and alteration were at 250 to 460 °C and 1 to 3.7 kbar, but cluster at 250 to 380 °C and 1 to 3 kbar for the main gold mineralization in stages 2 and 3. The retrograde P-T evolution was produced by uplifting and cooling.

4. The $\delta^{13}C$ values of late stage 4 vein carbonates range from -6.3 and -2.5‰; the $\delta^{13}C$ values of fluid inclusion CO_2 in vein quartz from stages 1 to 3 span a range from -6.1 to -4.3‰. The $\delta^{34}S$ values of sulphides range from 2.6 to 6.3‰. These are consistent with isotopic compositions of magmaitc-derived sulphur and carbon.

5. The $\delta^{18}O$ values from alteration-zone quartz and sericite, vein quartz, K-feldspar and carbonates range from 8.4 to 15.8‰; the estimated $\delta^{18}O_{H2O}$ values from quartz are between 3.9 and 7.2‰. The measured δD values of alteration-zone sericite cluster at -51 to -45‰, corresponding to the δD_{H2O} values of -26 and -20‰ at 350 ± 50 °C; the measured δD values of fluid inclusions in vein quartz from stages 1 to 3 range from -85 to -64‰. These suggest that the mineralizing fluids were mainly derived from magmas. The calculated O-H isotope water/rock exchange indicate that meteoric waters were mixed to a small degree with the ore-forming fluids.

6. It is suggested that the $Au(HS)_2^-$ complex dominates in the fluids. The gold precipitation was mainly caused by cooling of the ore-bearing fluids and the sulphidization of the wall rocks which caused sulphur activities in the fluids to decrease.

7. On the basis of geological and geochemical characteristics, fluid inclusions and stable isotopes of the ores, a genetic model is proposed which suggests that the Niuxinshan gold deposit was derived from magmatic fluids that were partially mixed with meteoric waters.

ACKNOWLEDGMENTS

This paper forms part of the senior author's PhD dissertation. He gratefully acknowledges the DAAD (German Academic Exchange Service) for financial support of his PhD study in Germany and wishes to thank Drs. G. Grundmann, L. Hecht, G. Lehrberger, R. Wiesheu, S. Schödlbauer, Dipl.-Geol. Ch. Preinfalk, Dipl.-Geol. T. Herzog, Mr. R. Beiderbeck, Mrs. K. Holzhäuser, Mr. V. Ruttner, Miss I. Claus, and Mrs. Ch. Hochschulte in the Institute for Applied Mineralogy and Geochemistry, Technical University of Munich; and Dr. D. Blamart (now Centre des Faibles Radioactivités, France) for all the help related to academic problems and practical matters during his stay in the Institute. Dr. B. J. Zhao (Wits University, Johannesburg) is thanked for suggestions to improve the manuscript. Finally, Prof. C. R. Anhaeusser is gratefully acknowledged for his constructive comments on the manuscript.

REFERENCES

Bai, H. S., Gu, M. Z. and Chen, J. F. (1990) Research report on gold metallogenic model and prognosis in eastern Hebei and southern inner Mongu, China (in Chinese). The First Geological Exploration Co., Ministry of Metallurgical Industry, Beijing, 355 pp.

Barnes, H. L. (1979) Solubilities of ore minerals. In: Barnes, H. L. (ed.) Geochemistry of Hydrothermal Ore Deposits. New York, John Wiley, 404-460.

Bigeleisen, J., Perlman, M. L. and Prosser, H. C. (1952) Conversion of hydrogenic materials to hydrogen for isotopic analysis. Analytical Chem. **24**: 1356-1357.

Bottinga, Y. (1968) Calculation of fractionation factors for carbon and oxygen isotopic exchange in the system calcite-carbon dioxide-water. J. Phy. Chem., **72**, 800-808.

Boyle, R. W. (1979) The geochemistry of gold and its deposits. Bull. Geol. Surv. Canada **280**, 584 pp.

Briqueu, L., Bougault, H. and Joron, J. L. (1984) Quantification of Nb, Ta, Ti, and V anomalies in magmas associated with subduction zones: petrogenetic implications. Earth Planet. Sci. Lett. **68**: 297-308.

Burrows, D. R. and Spooner, E. T. C. (1987) Generation of a magmatic H_2O-CO_2 fluid enriched in Mo, Au, and W within an Archean sodic granodiorite stock, Mink Lake, northwestern Ontario. Econ. Geol. **82**: 1931-1957.

Burrows, D. R., Wood, P. C. and Spooner, E. T. C. (1986) Carbon isotope evidence for a magmatic origin for Archean gold-quartz vein ore deposits. Nature **321**: 851-854.

Cassidy, K. F. and Bennett, J. M. (1993) Gold mineralization at the Lady Bountiful Mine, Western Australia: an example of a granitoid-hosted Archean lode gold deposit. Mineral. Deposita 28: 388-408.

Chacko, T., Hu, X. S., Mayeda, T. K., Clayton, R. N. and Goldsmith J. R. (1995) Oxygen isotope fractionations in muscovite, phlogopite, and rutile. Geochim. Cosmochim. Acta **60**: 2595-2608.

Chappell, B. W. and White A. J. R. (1992) I- and S-type granites in the Lachlan Fold Belt. Trans. R. Soc. Edinburgh, Earth Sci. **83**: 1-26.

Clayton, R. N. and Mayeda, T. K. (1963) The use of bromine pentafluoride in the extraction of oxygen from oxides and silicates for isotopic analysis. Geochim. Cosmochim. Acta **27**: 43-52.

Criss, R. E. and Taylor, H. P. Jr. (1986) Meteoric hydrothermal systems. In: Valley, J. W., Taylor, H. P. and O'Neil, J. R. (eds.) Stable Isotopes in High Temperature Geological Processes. Reviews in Mineralogy **16**: 373-424.

Dada, S. S., Briqueu, L., Harms, U., Lancelot, J. R. and Matheis, G. (1995) Charnockitic and monzonitic Pan-African series from north-central Nigeria: Trace element and Nd, Sr, Pb isotope constraints on their petrogenesis. Chem. Geol. **124**: 233-252.

De Ronde, C. E. J., Spooner, E. T. C., De Wit, M. J. and Bray, C. (1992) Shear zone-related, Au quartz-vein deposits in the Barberton greenstone belt, South Africa: Field and

petrographic characteristics, fluid inclusion properties, and light stable isotope geochemistry. Econ. Geol. **87**: 366-402.

Diamond, L. W. (1990) Fluid inclusion evidence for P-V-T-X evolution of hydrothermal solutions in Late-Alpine gold-quartz veins at Brusson, Val D'Ayas, Northwest Italian Alps. Am. J. Sci. **290**: 912-958.

Doe, B. R. and Zartman, R. E. (1979) Plumbotectonics, the Phanerozoic. In: Barnes, H. L. (ed.) Geochemistry of Hydrothermal Ore Deposits. John Wiley & Sons, New York, 22-70.

Groves, D. I. and Foster, R. P. (1991) Archean lode gold deposits. In: Foster, R. P. (ed.) Gold Metallogeny and Exploration. Blackie, London, 63-103.

Groves, D. I., Goldfarb, R. J., Gebre-Mariam, M., Hagemann, S. G. and Robert, F. (1998) Orogenic gold deposits: A proposed classification in the context of their crustal distribution and relationship to other gold deposit. Ore Geol. Rev. **13**: 7-27.

Hattori, K. (1987) Magnetic felsic intrusion associated with Canadian Archean gold deposits. Geology **15**: 1107-1111.

Hayashi, K. I. and Ohmoto, H. (1991) Solubility of gold in NaCl- and H_2S-bearing aqueous solutions at 250-350 °C. Geochim. Cosmochim. Acta **55**: 2111-2126.

Hedenquist, J. W. and Lowenstern, J. B. (1994) The role of magmas in the formation of hydrothermal ore deposits. Nature **370**: 519-527.

Hedenquist, J. W., Izawa, E., Arribas, A. and White, N. C. (1996) Epithermal gold deposits: Styles, characteristics, and exploration. Res. Geol. Spec. Publ. **1**: 16 pp.

Henley, R. W. (1973) The solubility of gold in hydrothermal chloride solutions. Chem. Geol. 11: 73-87.

Ho, S. E. (1987) Fluid inclusions: Their potential as an exploration tool for Archaean gold deposits. In: Ho, S. E. and Groves, D. I. (eds.) Recent advances in understanding Precambrian gold deposits. I. Univ. West. Aust. Geol. Dept. & Univ. Exten. Publ. **11**: 239-263.

Jahn, B. M., Auvray, B., Blais, S., Capdevila, R., Cornichet, J., Vidal, F. and Hameurt, J. (1980) Trace element geochemistry and petrogenesis of Finnish greenstone belts. J. Petrol. **21**: 210-244.

Kay, A. and Strong, D. F. (1983) Gological and fluid controls on As-Sb-Au mineralization in the Moretons Harbour area, Newfoundland. Econ. Geol. **78**: 1590-1604.

Kerrich, R. (1987) The stable isotope geochemistry of Au-Ag vein deposits in metamorphic rocks. Mineral Assoc. Can. Short Course Handbook **13**: 287-336.

Kerrich, R. (1993) Perspective on genetic models for lode gold deposits. Mineral. Deposita **28**: 362-365.

Liu, L. D. (1989) A new understanding of magmatic hydrothermal gold deposits. In: Guan, G. Y. and Zhu, F. S. (eds.,) Proc. Int. Symp. on Gold Geology and Exploration. 26-30 June, 1989, Shenyang. Northeast Univ. Technology Publ. House, Shenyang, 120-122.

Matsuhisa, Y., Goldsmith, J. R. and Clayton, R. N. (1979) Oxygen isotope fractionation in the system quartz-albite-anorthite-water. Geochim. Cosmochim. Acta **43**: 1131-1140.

McCrea, J. M. (1950) On the isotopic chemistry of carbonates and a Paleotemperature scale. J. Chem. Phys. **18**: 849-857.

McCuaig, T. C. and Kerrich, R. (1994) P-T-t-Deformation-fluid characteristics of lode gold deposits: Evidence from alteration systematics. In: Lentz, D. R. (ed.) Alteration and Alteration Processes Associated with Ore-forming Systems. Geol. Assoc. Can. Short Course Note **11**: 339-379.

Mikucki, E. J. and Ridley, J. R. (1993) The hydrothermal fluid of Archean lode-gold deposits at different metamorphic grades: compositional constraints from ore and wallrock alteration assemblages. Mineral. Deposita **28**: 469-481.

Miller, L. D., Goldfarb, R. J., Nie, F. J., Hart, C. J. R., Miller, M. L., Yang, Y. Q. and Liu, Y. Q. (1998) North China gold: A product of multiple orogens. SEG Newsletter **33**: 1; 6-12.

Nabelek, P. I. and Ternes, K. (1997) Fluid inclusions in the Harney Peak Granite, Black Hills, South Dakota, USA: Implications for solubility and evolution of magmatic volatiles and crystallization of leucogranite magmas. Geochim. Cosmochim. Acta **61**: 1447-1465.

Nesbitt, B, E. and Muehlenbachs, K. (1989) Geology, geochemistry, and genesis of mesothermal lode gold deposits of the Canadian Cordillera : evidence for ore formation from evolved meteoric water. Econ. Geol. Mono. **6**: 553-563.

O'Neil, J. R. and Chappell, B. (1977) Oxygen and hydrogen isotope relations in the Berridale batholith. J. Geol. Soc. London, **133**, 559-571.

Ohmoto, H. (1986) Stable isotope geochemistry of ore deposits. In: Valley, J. W., Taylor, H. P. and O'Neil, J. R. (eds.) Stable Isotopes in High Temperature Geological Processes. Reviews in Mineralogy **16**: 491-560.

Ohmoto, H. and Rye, R. O. (1979) Isotopes of sulfur and carbon. In: Barnes, H. L. (ed.) Geochemistry of Hydrothermal Ore Deposits. John Wiley & Sons, New York, 509-567.

Pearce, J. A., Harris, N. B. W. and Tindle, A. G. (1984) Trace element discrimination diagrams for the tectonic interpretation of granitic rocks. J. Petrol. **25**: 956-983.

Roedder, E. (1963) Studies of fluid inclusions II: Freezing data and their interpretation. Econ. Geol. **58**: 167-211.

Rösler, H. J. and Lange, H. (1972) Geochemical Tables. Elsevier Publishing Co.,Amsterdam, 468 p.

Seward, T. M. (1973) Thio complexes of gold and the transport of gold in hydrothermal ore solutions. Geochim. Cosmochim. Acta **37**: 370-399.

Seward, T. M. (1984a) The formation of lead (II) chloride complexes to 300 °C: A spectrophotometric study. Geochim. Cosmochim. Acta **48**: 121-134.

Seward, T. M. (1984b) The transport and deposition of gold in hydrothermal systems. In: Foster, R. P. (ed.) Gold'82, The Geology, Geochemistry and Genesis of Gold Deposits. A. A. Balkema, Rotterdam, 165-181.

Seward, T. M. (1991) The hydrothermal geochemistry of gold. In: Foster, R. P. (ed.) Gold Metallogeny and Exploration. Blackie, London, 37-62.

Shelton, K. L., So, C. S. and Chang, J. S. (1988) Gold-rich mesothermal vein deposits of the Republic of Korea: Geochemical studies of the Jungwon gold area. Econ. Geol. **83**: 1221-1237.

Shenberger, D. M. and Barnes, H. L. (1989) Solubility of gold in aqueous solutions from 150 to 350 °C. Geochim. Cosmochim. Acta 53: 269-278.

Sheppard, S. M. F. and Gilg, H. A. (1996) Stable isotope geochemistry of clay minerals. Clay Minerals **31**: 1-24.

Sillitoe, R. H. (1989) Gold deposits in Western Pacific island arcs, the magmatic connection. Econ. Geol. Mono. **6**: 274-291.

Sillitoe, R. H. (1991) Intrusion-related gold deposits. In: Foster, R. P. (ed.) Gold Metallogeny and Exploration. Blackie, London, 165-209.

So, C. S., Yun, S. T. and Shelton, K. L. (1995) Mesothermal gold vein mineralization of the Samdong mine, Youngdong mining district, Republic of Korea. Mineral. Deposita **30**: 384-396.

Solomon, M. and Groves, D. I. (1994) The geology and origin of Australia's mineral deposits. Oxford Sci. Publ., 951 pp.

Spooner, E. T. C. (1991) The magmatic model for the origin of Archean Au-quartz vein ore system: an assessment of the evidence. In: Ladeira, E. A. (ed.) Brazil Gold'91, Rotterdam, Balkema, 313-318.

Streckeisen, A. (1976) To each plutonic rock its proper name. Earth Sci., Rev. **12**: 1-33.

Sun, D. Z., Wang, K. Y., Wang, J. L., Yang, C. L. and Zhao, F. M. (1989) Studies on auriferous rock series of Archean in eastern Hebei Province. In: Contributions to the project of regional metallogenetic conditions of main gold deposit types in China: eastern Hebei Province (in Chinese with English summary). Geol. Publ. House, Beijing, 49-89.

Sun, S. S. (1980) Lead isotopic study of young volcanic rocks from mid-ocean ridges, ocean islands and island arcs. Phil. Trans. R. Soc. Lond., **A 297**, 409-445.

Taylor, B. E. (1986) Magmatic volatiles: isotopic variation of C, H, and S. In: Valley, J. W., Taylor, H. P. and O'Neil, J. R. (eds.) Stable Isotopes in High Temperature Geological Processes. Rev. Mineralogy **16**: 185-225.

Taylor, H. P. (1977) Water/rock interactions and the origin of H_2O in granitic batholiths. J. Geol. Soc. Lodon, **133**, 509-558.

Thiéry, R., Martinus, V. D. K. and Dubessy, J. (1994) vX properties of CH_4-CO_2 and CO_2-N_2 fluid inclusions: modelling for T <31°C and P <400 bars. Eur. J. Mineral. **6**: 753-771.

Trumbull, R. B., Morteani, G., Lehrberger, G. and Satir, M. (1996) Gold deposits and Mesozoic granites in NE China. Geowiss. **14**: 325-328.

Trumbull, R. B., Morteani, G., Li, Z. L. and Bai, H. S. (1992) Gold Metallogeny in the Sino-Korean Platform. Springer-Verlag, Berlin, 202 pp.

Whalen, J. B. and Currie, K. L. (1990) The Topsails igneous suite, western Newfoundland; fractionation and magma mixing in an „orogenic" A-type granite suite. In: Stein, H. J. and Hannah, J. L. (eds.) Ore-bearing Granite Systems; petrogenesis and mineralizing processes. Geol. Soc. Am. Spec. Paper, **246**, 287-299.

Witt, W. K., Knight, J. T. and Mikucki, E. J. (1997) A synmetamorphic lateral fluid flow model for gold mineralization in the Archean Southern Kalgoorlie and Norseman Terranes, Western Australia. Econ. Geol. **92**: 407-437.

Wyborn, D. and Sun, S. S. (1994) Sulphur-undersaturated magmatism: A key factor for generating magma-related copper-gold deposit. AGSO Res. Newsletter **21**: 7-8.

Yang, L. S. (1989) Endogenic gold metallogenesis in connection with deep-seated source and prospecting prediction. In: Guan, G. Y. and Zhu, F. S. (ed.) Proc. Int. Symp. on Gold Geology and Exploration. 26-30 June, 1989, Shengyang. Northeast Univ. Tech. Publ. House, Shengyang, 664-668.

Yao, Y. (1997) A mineralogical-geochemical, fluid inclusion and stable isotope study of gold ores in the Niuxinshan deposit, eastern Hebei, NE China: wall rock alteration and the role of granite in mineralization. Ph. D. thesis (unpubl.), Tech. Univ. Munich, 158 pp.

Yao, Y., Morteani, G. and Trumbull, R. B. (1999) Fluid inclusion microthermometry and the P-T evolution of gold-bearing hydrothermal fluids in the Niuxinshan gold deposit, eastern Hebei Province, NE China. Mineral. Deposita (in press).

Yu, C. T. and Jia, B. (1989) Study on the genesis of major types of gold deposits and its mechanism of formation in eastern Hebei. In: Contributions to the Project of Regional Metallogenetic Conditions of Main Gold Deposit Types in China: Eastern Hebei Province (in Chinese with English summary). Geol. Publ. House, Beijing, 1-48.

Yu, R. L., Li, W. L., Gu, S. Z., Li, J. L., Wang, F. Z., Zhao, W. H., Liu, S. and Zhang, H. X. (1989) Metallogenetic conditions of major gold ore types and ore-searching orientation in eastern Hebei. In: Contributions to the Project of Regional Metallogenetic Conditions of

Main Gold Deposit Types in China: Eastern Hebei Province (in Chinese with English summary). Geol. Publ. House, Beijing, 99-146.

Zartmen, R. E. and Doe, B. R. (1981) Plumbotectonics: the model. Tectonophysics 75: 135-162.

Zhang, Q. S., Yang, Z. S., Gao, D. Y. and Re, H. M. (1991) The Archaean high-grade metamorphic geology and gold deposits in Jinchangyu area of eastern Hebei (in Chinese). Geol. Publ. House, Beijing, 445 pp.

—— oOo ——